New iminodiacetate-thiosemicarbazone hybrids and their copper(II) complexes are potential ribonucleotide reductase R2 inhibitors with high antiproliferative activity

Mirela F. Zaltariov,[I,▽] Marta Hammerstad,[#] Homayon J. Arabshahi,[†] Katarina Jovanović,[‡] Klaus W. Richter,[§] Maria Cazacu,[▽] Sergiu Shova,[▽] Mihaela Balan,[▽] Niels H. Andersen,[¶] Siniša Radulović,[‡] Jóhannes Reynisson,[†] K. Kristoffer Andersson,[#] Vladimir B. Arion*,[I]

[I]*Institute of Inorganic Chemistry of the University of Vienna, Währinger Strasse 42, 1090 Vienna, Austria*

[▽]*"Petru Poni" Institute of Macromolecular Chemistry, Aleea G. Ghica Voda 41A, 700487, Iasi, Romania*

[#]*Section for Biochemistry and Molecular Biology, Department of Biosciences, University of Oslo, P.O. Box 1066, Blindern, NO-0316 Oslo, Norway*

[†]*School of Chemical Sciences, University of Auckland, New Zealand*

[‡]*Institute for Oncology and Radiology of Serbia, Pasterova 14, 11000 Belgrade, Serbia*

[¶] *Department of Chemistry, University of Oslo, P.O. Box 1033, Blindern, NO-0315 Oslo, Norway*

[§]*Institute of Inorganic Chemistry – Functional Materials, Althanstrasse 14, 1090 Vienna, Austria*

Abstract. As ribonucleotide reductase (RNR) plays a crucial role in nucleic acid metabolism, it is an important target for anticancer therapy. The thiosemicarbazone Triapine is an efficient R2-inhibitor, which has entered about 20 clinical trials. Thiosemicarbazones are supposed to exert their biological effects through effectively binding transition metal ions. In this study, six iminodiacetate-thiosemicarbazones able to form transition metal complexes, as well as six dicopper(II) complexes were synthesized and fully characterized by analytical, spectroscopic techniques (IR; UV–vis, ^{1}H and ^{13}C NMR), ESI mass spectrometry and X-ray diffraction. The antiproliferative effects were examined in several human cancer and one noncancerous cell lines. Several of the compounds showed high cytotoxicity and marked selectivity for cancer cells. Based on this, and on molecular docking calculations one lead dicopper(II) complex and one thiosemicarbazone were chosen for *in vitro* analysis as potential R2 inhibitors. Their interaction with R2 and effect on the $Fe(III)_2$-Y• cofactor were characterized by microscale thermophoresis, and two spectroscopic techniques, EPR and UV–vis spectroscopy. Our findings suggest that several of the synthesized proligands and copper(II) complexes are effective antiproliferative agents in several cancer cell lines, targeting RNR, which deserve further investigation as potential anticancer drugs.

Keywords: Copper(II) complexes, Iminodiacetate-thiosemicarbatone-hybrid, Anticancer, Ribonucleotide reductase, mouse R2 protein

Introduction

Thiosemicarbazones are well-known for their versatile coordination chemistry,[1] biological activity[2] and theranostic applications.[1a,3] 3-Amino-2-pyridinecarboxaldehyde thiosemicarbazone, also referred to as Triapine, a very efficient inhibitor of ribonucleotide reductase (RNR),[4] has entered a number of clinical trials[5,6,7] and showed promising results in treatment of hematological diseases.[8] However, low efficacy is detected in solid tumors,[9] presumably because of rapid development of resistance,[10] and, accompanied by marked side effects, e.g, methemoglobinemia.[5,6,7] RNRs catalyze the conversion of ribonucleotides to their corresponding deoxyribonucleotides in all living organisms, providing the essential building blocks required for DNA replication and repair.[11] The oxygen-dependent mammalian class Ia RNRs consist of two homodimeric subunits designated α_2 (R1) and β_2 (R2). A radical-based catalytic mechanism is operative in the R1 subunit, where nucleotide reduction is initiated through the reversible one-electron oxidation of a conserved cysteine residue to a thiyl radical. R2 houses a μ-oxo-bridged diferric tyrosyl radical (Fe^{III}_2-Y•) cofactor (Figure 1) essential for initiating thiyl radical formation in R1.[12] As RNR plays a crucial role in nucleic acid metabolism, it is target for several clinical drugs.[13] Triapine has been shown to be a potent inhibitor of the R2 subunit of RNR, and, insights into the underlying mechanisms were reported.[14] The understanding of, and the search for new compounds inactivating either the R1 or the R2 subunit of RNR is important for further optimization and development of new anticancer drugs.

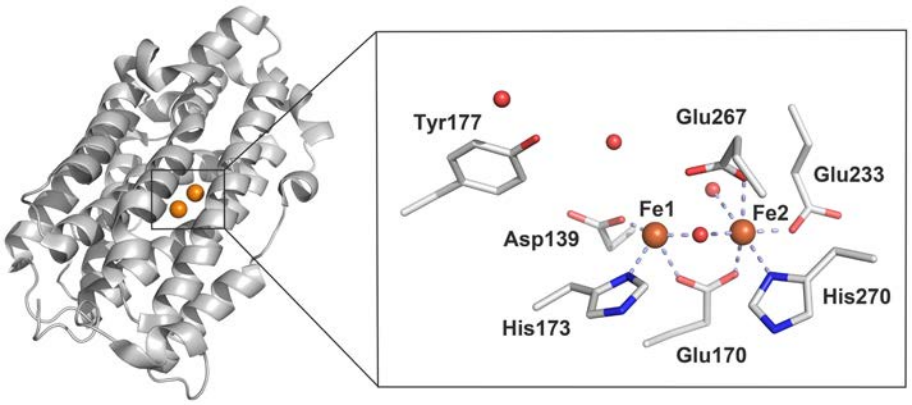

Figure 1. The RNR class Ia R2 subunit from mouse (PDBid:1W68).[15] The radical-generating subunit is displayed as a monomer (left). The inset panel on the right shows the metal ion site, where the Fe ions are shown as orange spheres, and the coordinating amino acids and Tyr are represented as sticks and colored by atom type.

Two thiosemicarbazones, (*E*)-*N*´-(6,7-dihydroquinolin-8(5*H*)-ylidene)-4-(pyridine-2-yl)piperazine-1-carbothiohydrazide (COTI-2), and di-2-pyridylketone 4-cyclohehyl-4-methyl-3-thiosemicarbazone (DpC) (Chart 1) have entered phase I clinical trials in 2016,[16,17] rekindling the interest in this class of

compounds and their metal complexes. COTI-2 is active against a large number of human tumor cell lines showing IC_{50} values in the nanomolar concentration range and also in xenografts.[18] It was found to be superior to some first-line chemotherapy drugs such as cisplatin and BCNU[19,20] or targeted-therapy agents, such as cetuximab and erlotinib.[21] DpC, a member of the second generation of di-2-pyridylketone thiosemicarbazone (DpT) analogues, was identified as a lead drug candidate.[22] It has shown a number of advantages over another lead compound, di-2-pyridylketone 4,4-dimethyl-3-thiosemicarbazone (Dp44mT), and, in particular higher antitumor activity *in vivo*, better tolerability when administered orally, lack of specific side-effects, and increased stability in blood plasma.[17,23]

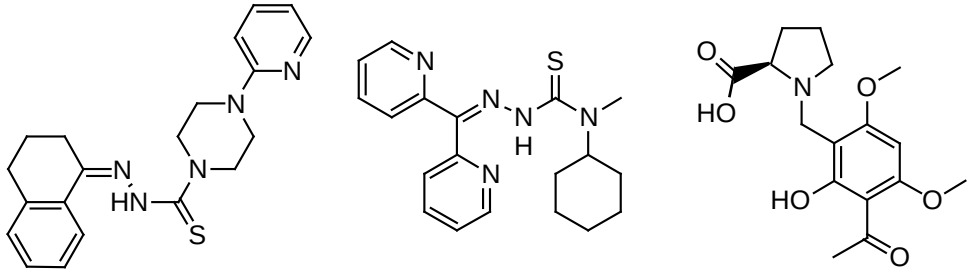

COTI-2 DpC (-)-monophylidin

Chart 1. Line drawings of thiosemicarbazones in clinical trials and of (–)-monophylidin.

Recently, we initiated synthesis of thiosemicarbazones originating from aldehydes closely related to (–)-monophyllidin (Chart 1),[24] a new alkaloid L-proline derivative from *Zanthoxilum monophillum*, which showed selective antibacterial activity against *Enterococcus faecalis* 29212, with the aim of increasing aqueous solubility and extending structure–cytotoxicity relationship studies. Note that investigation of thiosemicarbazones as potential anticancer agents in the 1950s followed the studies which demonstrated their antiviral activity.[25,26] L- and D-proline 5-methyl-salicylaldehyde thiosemicarbazones along with their copper(II) complexes were prepared and compared for antiproliferative activity *in vitro*.[27] The synthesis was further extended by replacing the phenolic moiety by a pyridine functionality,[28] since it was known that *N*-heterocyclic thiosemicarbazones with potential NNS binding sites for transition metals have increased antiproliferative activity both *in vitro* and *in vivo*.[17] Highly water-soluble copper(II) L- and D-proline 2-pyridinecarboxaldehyde thiosemicarbazones were found to act as inhibitors of topoisomerase IIα and display antiproliferative activity in CH1 ovarian carcinoma cells.[29]

Thiosemicarbazones exert their biological effects through the ability to effectively bind transition metal ions, in particular, iron(III).[30] Also, remarkable cell-dependent cytotoxicity of dicopper(II) and

dizinc(II) complexes with dinucleating ligands based on indolo[3,2-*c*]quinolines in A549 (nonsmall cell lung carcinoma), CH1 (ovarian carcinoma) and SW480 (colon adenocarcinoma) cell lines has been shown. Therefore, we decided to extend this last work on thiosemicarbazones by creating proligands able to form dimetal complexes, by including in their backbone a dialkyl-2,2´-iminodiacetate fragment (Chart 2). Incorporation of an iminodiacetate ligand into a dinuclear zinc(II) complex with phenanthroline was found favorable for inhibition of proliferation of hepatoma cell lines HepG2 and SMMC-7721, inducing cell cycle arrest in the G0/G1 phase. In addition, the complex showed low toxicity in mice (LD_{50} in ICR mice = 736 mg kg^{-1}).[31]

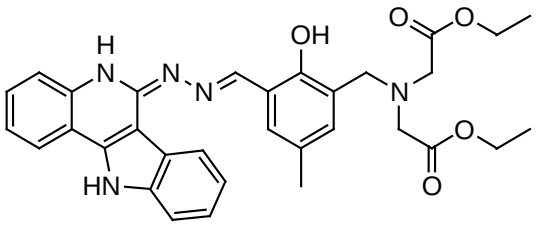

$^{EtOOC}HL^{COOEt}$

Chart 2. Line drawing of dinucleating indoloquinoline $^{EtOOC}HL^{COOEt}$.

Herein, to elucidate the structure–activity relationships (SARs), and to disclose their potential as R2 RNR inhibitors, we synthesized and characterized six proligands (Chart 3) by exploring the essential SAR derived from previous studies, in which the replacement of the terminal hydrogens by one or two alkyl group increased the cytotoxicity[23,10] and six dicopper(II) complexes (Chart 4). One lead dicopper(II) complex and one thiosemicarbazone were found to be able to bind to the protein with low μM affinities, as well as having a noticeable effect on the R2 tyrosyl radical (Y•) species as shown by using EPR and UV–vis spectroscopy. The utility of these methods along with rRaman spectroscopy in the studies of functional models of tyrosinase and galactose oxidase is well documented in the literature.[32,12]

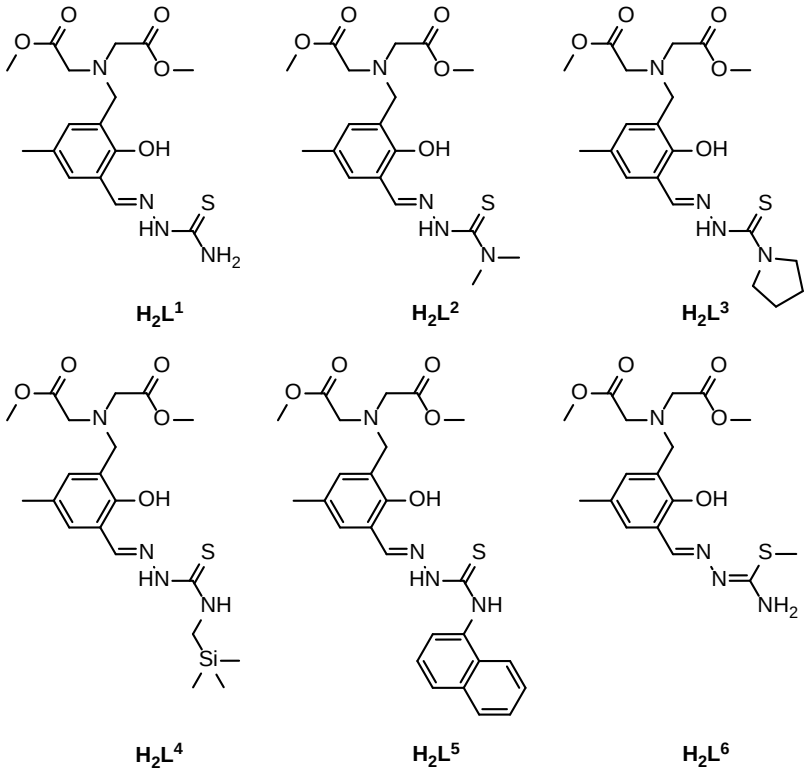

Chart 3. Proligands studied in this work. All compounds have been investigated by X-ray crystallography.

$[Cu_2(HL^1)Cl_3]$	(**1**)	$[Cu_2(HL^4)Cl_3]$	(**4**)
$[Cu_2(L^2)(OMe)]$	(**2**)	$[Cu_2(HL^5)Cl_3]$	(**5**)
$[Cu_2(L^3)(OMe)]$	(**3**)	$[Cu_2(L^6)Cl_3]$	(**6**)

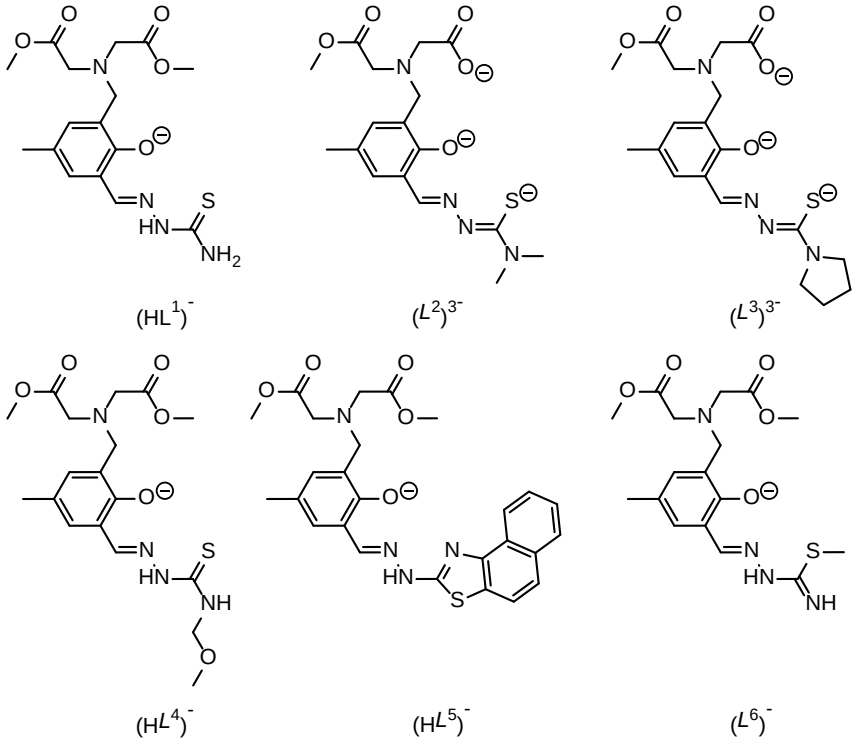

Chart 4. Copper(II) complexes studied in this work with line drawings for the ligands. All copper(II) complexes have been investigated by X-ray crystallography.

Results and Discussion

Syntheses. From the reaction of 3-(chloromethyl)-2-hydroxy-5-methylbenzaldehyde (species **A** in Scheme S1)[33] with dimethyliminodiacetate hydrochloride in THF/DCM 1:1 in the presence of triethylamine, the aldehyde **B** (Scheme S1) was prepared in 83% yield. The latter was further reacted with a series of substituted 4*N*-thiosemicarbazides to give six new thiosemicarbazones, $\mathbf{H_2L^1}$–$\mathbf{H_2L^6}$ (Chart 3), with yields ranging from 76 to 93%. The identity and purity of the aldehyde **B** and proligands was confirmed by elemental analysis, ESI mass spectra, IR, UV–vis, ^{1}H and ^{13}C NMR spectra (see Tables 1 and S1, Experimental, Figures S1–S25), as well as by X-ray crystallography (vide infra). The positive ESI mass spectra of all six proligands in methanol showed strong peaks attributed to $[M + H]^+$ or $[M + Na]^+$ or to both ions (see Experimental). Starting from $CuCl_2{\cdot}2H_2O$ and $\mathbf{H_2L^1}$, and by using methanol as a solvent at 50–60 °C, complexes **1**$\cdot 2H_2O$, **4**, **5** and **6**$\cdot 0.5H_2O$ (Chart 4) were prepared with yields ranging from 19 to 63%. The reaction of $Cu(OAc)_2{\cdot}H_2O$ with $\mathbf{H_2L^2}$ and $\mathbf{H_2L^3}$ in methanol at room temperature afforded **2** and **3** (Chart 4) in 25 and 41% yield, respectively. The formation of dicopper(II) complexes **1**–**4** was confirmed by positive ion ESI mass spectra. X-ray crystallographic studies (vide infra) revealed that upon complex formation, four proligands underwent chemical transformations. Thus, in the presence of copper(II) acetate one of the two ester groups of proligands $\mathbf{H_2L^2}$ and $\mathbf{H_2L^3}$ hydrolyzed with formation of carboxylic function enabling its coordination to copper(II). Upon reaction of copper(II) chloride with $\mathbf{H_2L^4}$, the –$SiMe_3$ group was replaced by –OMe originating from the solvent. Trimethylsilyl is generally known as a protecting group, which can then be easily cleaved by acid or base hydrolysis or by treating with fluoride ion. But, as compared to trimethylsilyl-oxygen, the trimethylsilyl-carbon bond is more hydrolytically stable surviving in a variety of synthetic transformations of the compounds, in which it is incorporated. However, the C−Si bond can be cleaved by electrophilic or nucleophilic agents. Both protic acids and Lewis acidic metal halides can be used as electrophiles.[34] It has been documented that this bond is also cleaved under mild conditions, e.g., in methanol in the presence of potassium carbonate[35] or potassium hydroxide,[36] silver nitrate in aqueous alcohol[37] and palladium salts.[38] In our case it would be assumed that copper(II) assists this replacement as a Lewis acidic metal center. In the presence of the same salt, an intramolecular cyclization via C–S coupling reaction between naphthyl carbon and thione group occurred in $\mathbf{H_2L^5}$ with formation of a five-membered thiaza ring. The generated group is of great interest in bioactive systems.[39] Only tautomeric changes were noticed upon complex formation between $CuCl_2$ and $\mathbf{H_2L^6}$. Nevertheless, we marked this modification by using an italic *L* for the ligand, as was also the case for the other four new ligands formed upon complex formation (see Chart 4). The IR spectra of the complexes showed

the blueshifted azomethine and carbonyl ester group vibrations as a result of coordination of Cu(II) ions by N and O donor atoms (Table 1 and Figures S26–S31).

Table 1. Assignment of the main characteristic bands in the IR spectra of the proligands and complexes **1**–**6**.

Assignment	**Wavenumber (cm^{-1})**												
	B	**H_2L^1**	**H_2L^2**	**H_2L^3**	**H_2L^4**	**H_2L^5**	**H_2L^6**	**1**	**2**	**3**	**4**	**5**	**6**
υ(O–H)	3290	3448	3445	-	-	3331	3456	3556	-	-	3441	-	-
$\upsilon(NH_2)$	-	3335	-	-	-	-	3344	3394	-	-	-	-	3304
υ(N–H)	-	3165	3306	3290	3325	3209	3124	3264	3290	3294	3180	3225	3177
$\upsilon(C–H)_{aromatic}$	3015	3024	3030	3084	3009	3045	2999	3015	3009	3026	3060	3078	3026
$\upsilon(C–H)_{aliphatic}$	2945	2953	2924	2947	2955	2955	2951	2953	2930	2966	2968	2949	2955
	2874	2916	2856	2862	2901	2885	2864	2918	2876	2868	2935	2916	2924
$\upsilon(C=O)_{ester}$	1740	1730	1724	1726	1732	1720	1736	1713	1720	1726	1720	1720	1726
$\upsilon(C=O)_{aldehyde}$	1674	-	-	-	-	-	-	-	-	-	-	-	-
$\upsilon_{as}(COO^-)$	-	-	-	-	-	-	-	-	1664	1659	-	-	-
$\upsilon_{s}(COO^-)$	-	-	-	-	-	-	-	-	1446	1448	-	-	-
υ(CH=N)	-	1595	1616	1616	1607	1597	1610	1566	1562	1564	1570	1547	1553
$\upsilon_{thioamide\ I\text{-}IV}$	-	1535	1547	1551	1529	1531	1524	1460	1510	1487	1535	-	1443
		1452	1450	1460	1480	1487	1460	1433	1414	1393	1456		1366
		1379	1379	1358	1329	1373	1377	1344	1342	1329	1391		1323
		835	845	868	820	868	864	814	822	822	812		862
$\upsilon_{thiazole\ ring}$	-	-	-	-	-	-	-	-	-	-	-	1481	-
												1443	
												1377	
												1319	
υ(N–N)	-	957	951	941	953	957	972	968	955	962	962	955	972
υ(C–N)	1269	1286	1292	1296	1294	1288	1288	1271	1268	1273	1283	1290	1294
$\upsilon(S–CH_3)$	-	-	-	-	-	-	726	-	-	-	-	-	729
$\upsilon(O–CH_3)$	-	-	-	-	-	-	-	-	-	-	2820	-	-
											1074		
$\upsilon(Si–CH_3)$	-	-	-	-	1246	-	-	-	-	-	-	-	-
					847								

The electronic absorption spectra of complexes in methanol showed the presence of broad and intense bands attributed to LMCT transitions at 374, 376, 375, 380, 417, and 370 nm, and to d-d transitions with maxima at 660, 638, 638, 634, 696 and 658 nm for **1**−**6**, respectively. All six complexes were found to crystallize from methanol with formation of X-ray diffraction quality

single crystals, which were investigated by X-ray crystallography (vide infra). In the case of **1** and **5**, the identity of single crystals with bulk samples was verified by powder diffraction measurements through the comparison to the calculated from single crystal X-ray data diffractograms (see Figures S32 and S33).

X-ray crystallography. The results of X-ray diffraction studies of proligands $\mathbf{H_2L^1}$–$\mathbf{H_2L^6}$ are shown in Figure 2, while those of complexes **1**–**6** in Figures 3 and 4. All six ligands act as binucleating accommodating two copper(II) ions. The ion Cu1 in complexes **1**, **4** and **6** adopts distorted square-pyramidal coordination geometry with calculated τ descriptor[40] of 0.30, 0.35 and 0.21, respectively, while in **5** the τ descriptor of 0.60 indicates a slow tendency towards a trigonal-bipiramidal environment around Cu1. The five coordination places surrounding Cu1 in **1** and **4** are occupied by ONS donor atoms, while in **5** and **6** by ONN donor atoms of the thiosemicarbazone moiety. In addition, in all four complexes, two chlorido ligands are bound to Cu1, one of which acts as bridging one to Cu2. The coordination environment of Cu2 is shown as four, five or six-coordinate with phenolato oxygen atom O1, iminediacetate nitrogen N4 and two chloride ligands Cl2 and Cl3 in equatorial plane, with no or very weakly coordinated apical or axial iminodiacetate oxygen atoms (see Figure 3 (a-d)). However, taking into account the corresponding interatomic distances the coordination environment at Cu2(Cu2a) should be described as six-coordinate in all four cases with weak axial binding of iminodiacetate oxygen atoms (see legend to Figure 3).

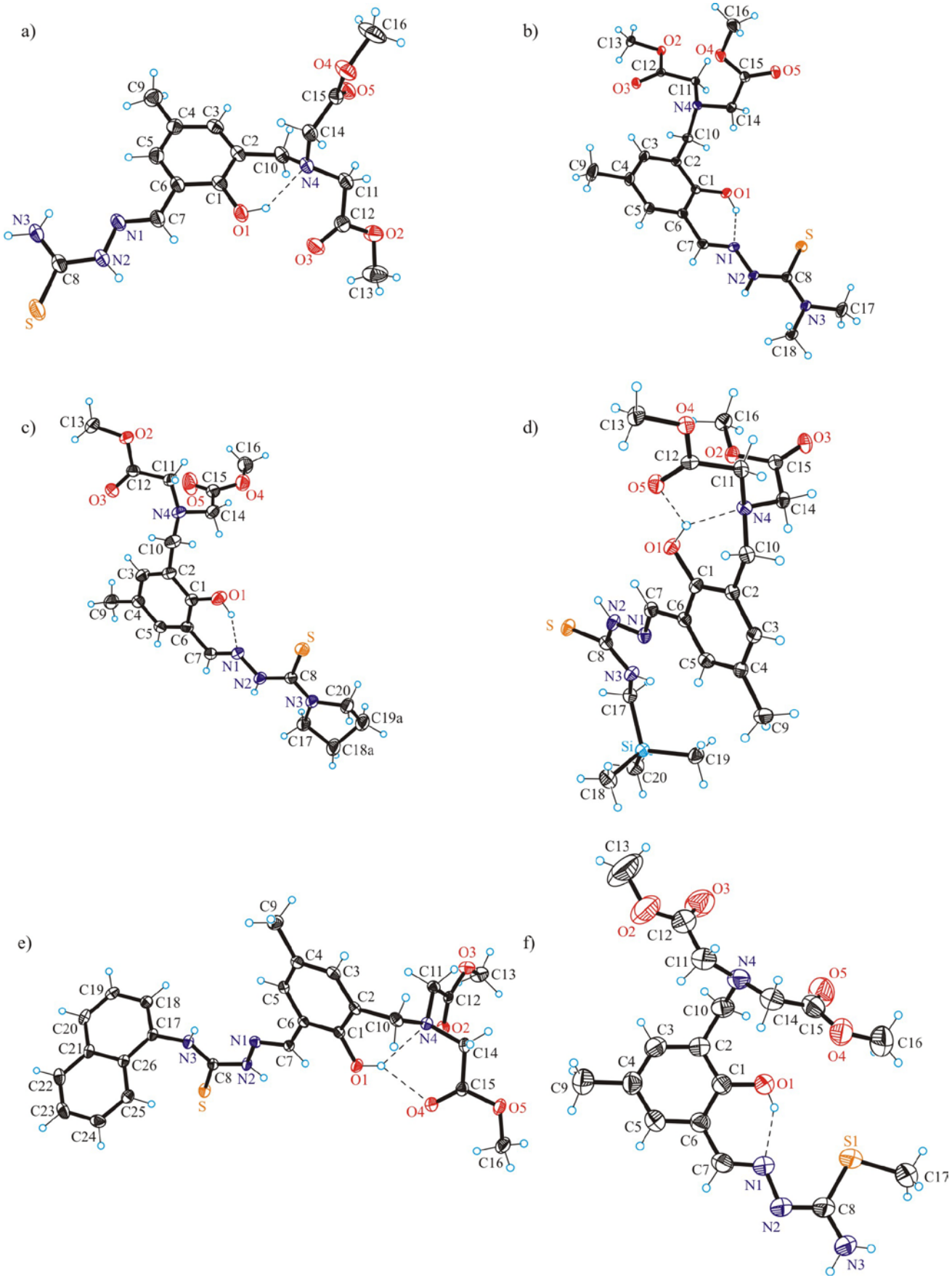

Figure 2. ORTEP views of a) H_2L^1, b) H_2L^2, c) H_2L^3, d) H_2L^4, e) H_2L^5 and f) H_2L^6.

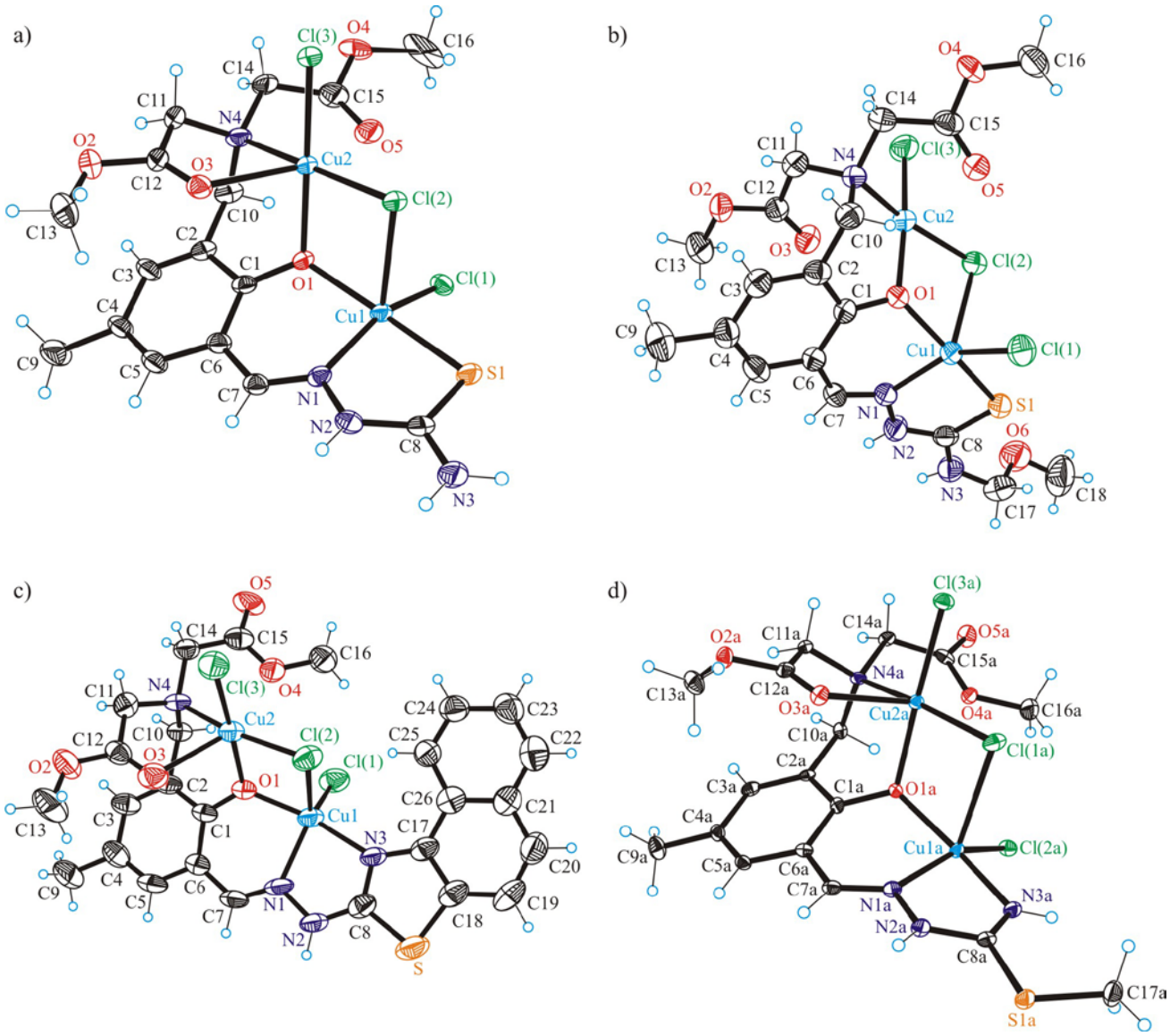

Figure 3. ORTEP views of a) **1**, b) **4**, c) **5** and d) **6**. Selected bond lengths and bond angles in **1**: Cu1–O1 1.984(3), Cu1–N1 1.990(4), Cu1–S1 2.2641(14), Cu1–Cl(1) 2.2652(12), Cu1–Cl(2) 2.6162(13), Cu2–O1 2.027(3), Cu2–N4 2.093(4), Cu2–Cl(2) 2.2853(13), Cu2–Cl(3) 2.2641(13), Cu2–O3 2.383(3), Cu2–O5 2.438(4) Å; O3–Cu2–O5 151.61(13), Cu1–O1–Cu2 110.76(16), Cu1–Cl(2)–Cu2 84.37(4)°; in **4**: Cu1–O1 1.979(2), Cu1–N1 1.982(3), Cu1–S1 2.2862(10), Cu1–Cl(1) 2.2717(10), Cu1–Cl(2) 2.5684(10), Cu2–O1 2.016(2), Cu2–N4 2.099(3), Cu2–Cl(2) 2.2962(10), Cu2–Cl(3) 2.2324(10), Cu2–O3 2.468(3), Cu2–O5 2.556(3) Å; O3–Cu2–O5 148.65(9), Cu1–O1–Cu2 112.43(11), Cu1–Cl(2)–Cu2 85.92(3)°; in **5**: Cu1–O1 1.937(4), Cu1–N1 2.024(4), Cu1–N3 2.029(4), Cu1–Cl(1) 2.2565(16), Cu1–Cl(2) 2.5667(15), Cu2–O1 2.012(3), Cu2–N4 2.079(4), Cu2–Cl(2) 2.2614(15), Cu2–Cl(3) 2.2451(15), Cu2–O3 2.390(4), Cu2–O4 2.555(4) Å; O3–Cu2–O5 149.26(14), Cu1–O1–Cu2 111.85(17), Cu1–Cl(2)–Cu2 85.06(5)°; in **6**: Cu1a–O1a 1.955(3), Cu1a–N1a 1.999(3), Cu1a–N3a 1.957(3), Cu1a–Cl(1a) 2.6357(12), Cu1a–Cl(2a) 2.2367(10), Cu2a–O1a 2.013(3), Cu2a–N4a 2.088(3), Cu2a–Cl(1a) 2.2753(11), Cu2a–Cl(3a) 2.2692(11), Cu2a–O3a 2.363(3), Cu2a–O4a 2.512(3) Å; O3–Cu2–O5 148.95(12), Cu1a–O1a–Cu2a 114.62(13), Cu1a–Cl(1a)–Cu2a 85.37(4)°.

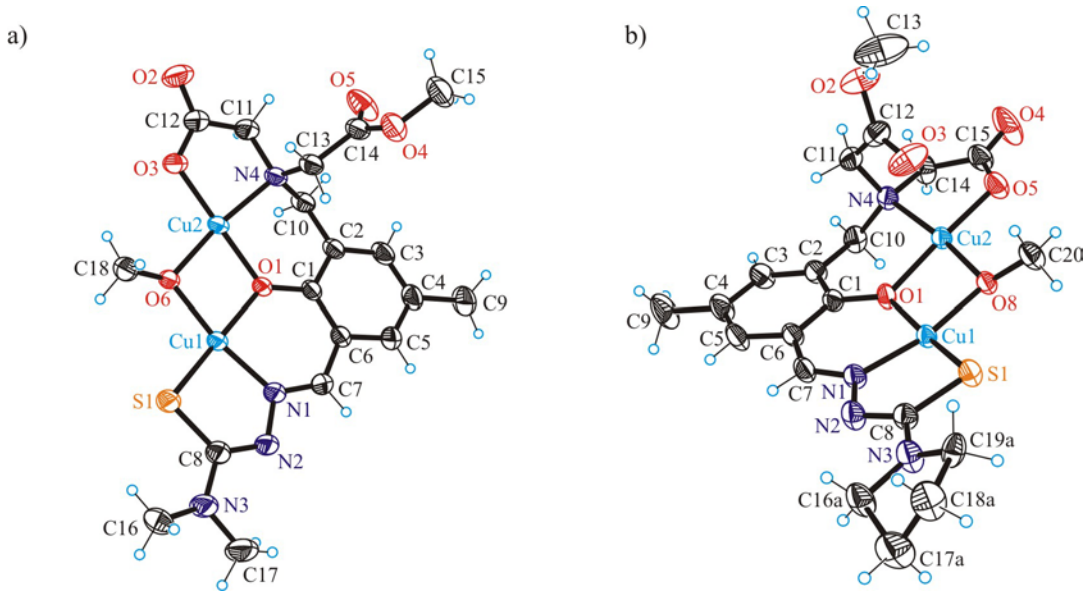

Figure 4. ORTEP views of compounds a) **2** and b) **3**. Selected bond lengths and bond angles in **2**: Cu1–O1 1.9605(11), Cu1–N1 1.9330(14), Cu1–S1 2.2340(4), Cu1–O6 1.9439(11), Cu2–O1 1.9376(11), Cu2–N4 2.0109(13), Cu2–O3 1.8978(12), Cu2–O6 1.9287(10) Å; Cu1–O1–Cu2 99.63(5), Cu1–O6–Cu2 100.53(5)°; in **3**: Cu1–O1 1.9619(13), Cu1–N1 1.9417(16), Cu1–S1 2.2411(5), Cu1–O8 1.9569(12), Cu2–O1 1.9527(13), Cu2–N4 2.0171(16), Cu2–O5 1.9170(14), Cu2–O8 1.9388(12) Å; Cu1–O1–Cu2 99.98(6), Cu1–O8–Cu2 100.64(6)°.

In complexes **2** and **3**, ligands $(L^2)^{3-}$ and $(L^3)^{3-}$ and one bridging methoxido group provide square-planar environment around both Cu1 and Cu2. Further inspection of the crystal structures revealed formation of tetranuclear associates via centrosymmetric intermolecular contacts Cu2–S1^{i} and Cu1–O6^{i}(methoxido) (see Figures S34 and S35), so that the coordination geometry should be described as square-pyramidal for both Cu1 and Cu2 (τ descriptor 0.01 and 0.04 for **2** and **3**, respectively).

MTT assay. Cytotoxic activity of the investigated copper(II) complexes **1**–**6** and cisplatin (CDDP) as standard cytotoxic agent was determined by the MTT assay after 48 h treatment of four tumor cell lines (HeLa, A549, K562, LS-174) and one normal cell line (MRC-5). The results are shown in Table 2. Mean IC_{50} values were calculated from two to three independent experiments and presented with their standard deviations.

Results of this assay indicate that most of the investigated complexes and the corresponding proligands exhibit moderate to strong cytotoxic activity towards all tested cell lines, comparable or even stronger than cisplatin.

Comparison of cytotoxic activity of the complexes with their corresponding proligands shows that complexation with copper(II) may have a different impact on the cytotoxicity properties of these types of compounds. For the **1** − $\mathbf{H_2L^1}$ and **5** − $\mathbf{H_2L^5}$ complex-proligand pairs, introducing a copper center into the organic ligand results in significant increase in cytotoxic activity in all investigated cell lines. The most prominent increase in cytotoxic activity is noted in the **5** − $\mathbf{H_2L^5}$ complex-proligand pair, with IC_{50} values not reached in the examined range of concentrations for the proligand, and with IC_{50} values of 14.4 ± 1.0, 14.9 ± 0.1 and 11.7 ± 0.4 μM on HeLa, A549 and LS-174 cell lines respectively, for **5** (Table 2). Besides increased cytotoxicity, the absence of selectivity towards cancer cell lines should be taken into account for the two complexes **1** and **5**.

Table 2. Results of MTT assay presented as IC_{50} (μM) values obtained after 48 h incubation.

	IC_{50} [μM] (mean ± SD)					**SI_1**[a]
compound	**HeLa**	**K562**	**A549**	**LS-174**	**MRC-5**	
1	3.7 ± 0.6	3.2 ± 0.1	4.3 ± 0.6	4.1 ± 0.3	5.7 ± 0.4	1.8
2	6.1 ± 0.4	3.8 ± 0.1	17.7 ± 1.0	12.6 ± 1.3	12.3 ± 1.4	3.2
3	21.0 ± 0.9	12.7 ± 1.3	95.5 ± 3.5	65.6 ± 2.0	>100	>7.9
4	5.5 ± 0.4	5.8 ± 0.4	13.1 ± 1.3	9.4 ± 0.1	11.0 ± 0.3	1.9
5	14.4 ± 1.0	16.1 ± 1.5	14.9 ± 0.0	11.7 ± 0.4	13.9 ± 0.1	0.9
6	6.0 ± 0.6	7.2 ± 0.7	9.3 ± 0.8	8.7 ± 0.1	13.0 ± 1.0	1.8
H_2L^1	31.1 ± 2.3	7.1 ± 0.5	45.5 ± 4.8	40.0 ± 2.8	>100	>14.1
H_2L^2	4.2 ± 0.3	4.8 ± 0.4	5.4 ± 0.0	4.7 ± 0.6	99.1 ± 0.4	20.7
H_2L^3	3.9 ± 0.2	6.1 ± 0.7	8.5 ± 0.3	4.7 ± 0.2	84.7 ± 3.6	13.9
H_2L^4	6.1 ± 0.7	5.9 ± 0.1	13.6 ± 1.5	14.5 ± 0.3	19.4 ± 1.2	3.3
H_2L^5	>100	27.5 ± 1.2	>100	>100	>100	>3.6
H_2L^6	15.6 ± 2.8	5.1 ± 0.5	31.9 ± 1.8	16.2 ± 0.2	20.7 ± 1.2	4.1
CDDP	5.2 ± 0.3	18.6 ± 3.3	26.2 ± 5.4	22.4 ± 7.2	12.1 ± 0.9	0.7

The sign > (in front of the maximum value of the concentration) indicates that IC_{50} value is not reached in the examined range of concentrations. [a]SI = Selectivity index; $SI_1 = IC_{50}(MRC\text{-}5)/IC_{50}(K562)$.

For the **3** − $\mathbf{H_2L^3}$ complex-proligand pair, after binding of the copper(II) to the thiosemicarbazone ligand, a major drop in the cytotoxic activity occurs (Table 2). IC_{50} values increase starting from twofold (6.1 ± 0.7 vs 12.7 ± 1.3 μM for K562 cell line), to above tenfold (8.5 ± 0.3 vs 95.5 ± 3.5 μM for A549 cell line, and 4.7 ± 0.2 vs 65.6 ± 2.0 μM for LS-174 cell line). Interestingly, exhibited proligand selectivity towards cancer cells decreases or disappears completely with the formation of **3**.

For the **2** − $\mathbf{H_2L^2}$, **6** − $\mathbf{H_2L^6}$, and **4** − $\mathbf{H_2L^4}$ complex-proligand pairs, introduction of the copper(II) center did not result in significant change in the cytotoxic activity. Proligand $\mathbf{H_2L^2}$ exhibits great μM on HeLa, K562, A549 and LS-174 cell lines, respectively, vs 99.1 ± 0.4 μM on the MRC-5 cell line. With the formation of **2**, the selectivity towards cancer cells seen by the corresponding proligand decreases or disappears completely, in a similar way as in **3**. However, this complex together with its corresponding proligand show cytotoxic activity stronger than that of cisplatin in most of the examined cancer cell lines, which is promising for further investigations.

It is well-known, that methylation of thiosemicarbazones at sulfur atom changes their mode of coordination to the majority of transition metals.[41] This can be a reason for the divergent effect of thiomethylation on antiproliferative activity of proligands and their dicopper(II) complexes, elucidated by comparison of the IC_{50} values of $\mathbf{H_2L^1}$ and $\mathbf{H_2L^6}$, as well as of **1** and **6**. Thiomethylated proligand $\mathbf{H_2L^6}$ is more cytotoxic than nonmethylated proligand $\mathbf{H_2L^1}$, while its copper(II) complex **6** is less active against cancer cell lines than **1**.

Copper(II) complexes with hydroxyquinoline 2-carboxaldehyde thiosemicarbazones showed antiproliferative activity in lung adenocarcinoma cancer cells A549 with IC_{50} values in submicromolar concentration range, which is by more than one order of magnitude higher than that of the corresponding metal-free thiosemicarbazones, associated with cell cycle arrest in the G_2/M phase. The complexes do not induce ROS accumulation in the cells and do not produce DNA damage.[42] In contrast, chemically induced DNA cleavage presumably via singlet oxygen and hydroxyl radical generation was documented for copper(II) complex with quinoline-2-carboxaldehyde thiosemicarbazone.[43] Copper(II) 2-hydroxybenzaldehyde thiosemicarbazonates were found to be significantly more cytotoxic in A549 cells than the corresponding metal-free thiosemicarbazones with IC_{50} values from 0.95 to 2.19 μM compared to 4.4 to 95.5 μM for **1**–**6**. At the same time the metal-free thiosemicarbazones are markedly less active than iminodiacetate-

thiosemicarbazone hybrids $\mathbf{H_2L^2}$, $\mathbf{H_2L^3}$, $\mathbf{H_2L^4}$ and $\mathbf{H_2L^6}$ studied in this work.[44] Flow cytometry showed a marked accumulation of the cells in S phase upon increasing the concentration of copper(II) complexes in human hepatoma BEL-7404 cells. The complexes induce apoptosis via the mitochondrial ROS generation. A similar mechanism of apoptosis was reported for copper(II) complexes with 2-pyridinecarboxaldehyde- and di(2-pyridyl)ketone thiosemicarbazones.[45] Related copper(II) complexes with 2-benzoylpyridine thiosemicarbazones showed antiproliferative activities in submicromolar concentration range and were more cytotoxic than the thiosemicarbazones themselves.[46] The underlying mechanism of antiproliferative activity of the copper(II) complexes is due to induced early apoptosis via ROS accumulation in the cells and DNA cleavage. Although some of the recently reported copper(II) complexes with thiosemicarbazones exhibit high antiproliferative activity in cancer cells, the reported data on selectivity for cancer cells are scarce.[47]

For further investigations compounds were selected from the series of proligands and dicopper(II) complexes based on their selectivity to cancer cells (see Table 2).

Cell cycle analysis. Cell cycle analysis of K562 cells treated with copper(II) complexes and their corresponding proligands **2** − $\mathbf{H_2L^2}$ and **3** − $\mathbf{H_2L^3}$, as well as with cisplatin was performed by flow cytometry after staining with propidium iodide.[48] Cells were continuously exposed to the investigated compounds and cisplatin for 24 and 48 h with concentrations corresponding to their IC_{50} values as shown in Table 2.

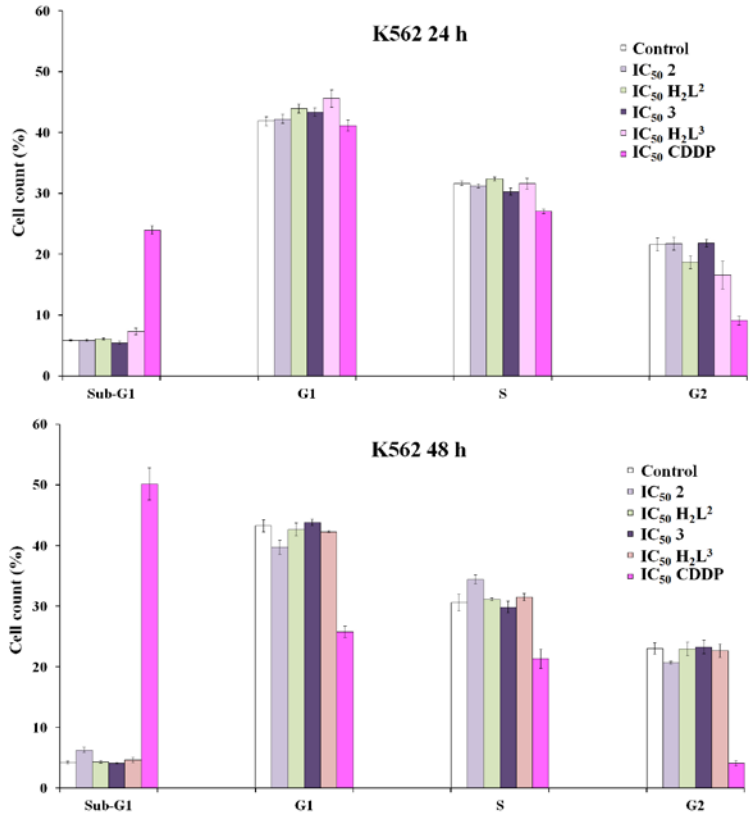

Figure 5. Effect of the investigated copper(II) complexes and cisplatin (CDDP) on cell cycle progression of K562 cells following 24 (upper chart) and 48 h (lower chart) incubation with concentrations of the investigated complexes corresponding to their IC_{50}s. Controls were untreated cells (incubated with nutrient medium only). The results are expressed as mean ± standard deviations of three independent experiments.

After 24 h of continuous treatment with the investigated compounds, only mild increase in the sub-G1 and G1 populations of the K562 cells treated with $\mathbf{H_2L^3}$ was noted, compared to the control population of cells. On the contrary, treatment with cisplatin, which was used as the positive control for this experiment, induced significant increase in the sub-G1 population of cells (Figure 5, upper chart).

After 48 h of continuous treatment there was an increase in the sub-G1 population of **2** treated cells, which may denote apoptotic and/or necrotic fraction of cells. Additionally, an S-phase arrest was also noticed, indicating possible binding of **2** to DNA of K562 cells. Further investigations regarding apoptotic potential of this complex was performed.

Apoptotic assay. Analysis of the apoptotic potential of **2** was investigated by flow cytometry dual staining of K562 cells with Annexin V-FITC and PI, method that enables detection of translocation of phosphatidylserine from the inner to the outer side of plasma membrane during apoptosis.

Results shown in Figure 6 indicate that after 48 h treatment with **2**, no increase in the number of cells labeled with Annexin V-FITC (early apoptotic), nor cells labeled with both dyes Annexin V-FITC and PI (late apoptotic and necrotic cells) was found, as compared to the control. However, after treatment with an IC_{50} concentration of complex **2**, the number of dead cells increased slightly, as compared to the control population (from 2.93 to 3.95%). A notable increase in percentage of dead cells is achieved after treatment with 1.5 × IC_{50} concentration of complex **2** (6.44% of dead cells). These results are in agreement with the results obtained from cell cycle analysis, where treatment with **2** induced an increase in the sub-G1 population of K562 cells (Figure 5). However, absence of early and late apoptotic populations of cells suggests that other mechanisms of cytotoxic activity are involved in the case of **2**.

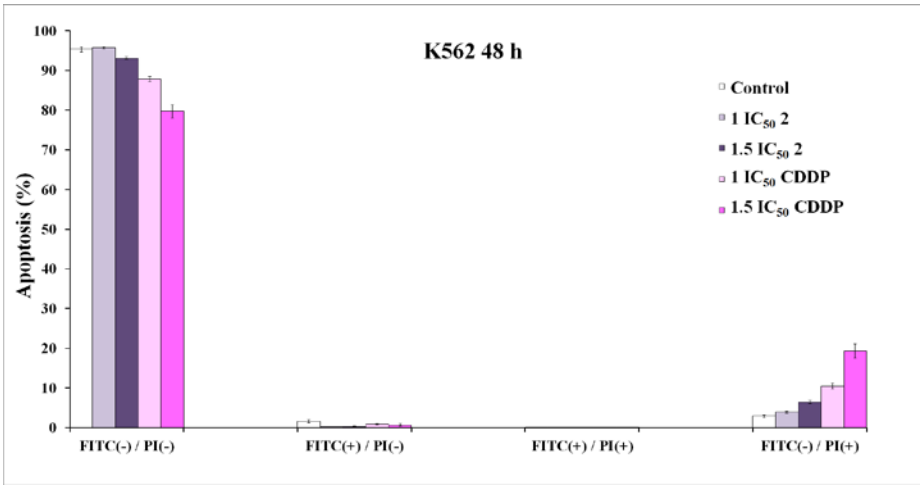

Figure 6. Apoptosis induction by complex **2** and CDDP. Cells were treated for 48 h with IC_{50} and 1.5 × IC_{50} concentrations of **2** and CDDP; FITC(-)/PI(-) are live cells, FITC(+)/PI(-) are early apoptotic cells, FITC(+)/PI(+) are late apoptotic or necrotic cells and FITC(-)/PI(+) are dead cells. The results are expressed as mean ± standard deviations of three independent experiments.

Molecular docking of RNR inhibitors – H_2L^2 and complex 3. To explain the findings from cytotoxicity assays and estimate the likelihood of binding to mouse R2 RNR, docking studies of R2 (PDBid:1W68) with the active compounds **H_2L^2** and **3** were conducted. The GoldScore (GS) scoring function was used to conduct the docking calculations, giving arbitrary numbers with higher values predicting better binding. Docking of copper(II) complex **3** resulted in a predicted pose across the binding pocket, the hydrophobic core was positioned deep in the pocket across several hydrophobic contacts (Figure 7). It gave a GS of 47 and predicted a single hydrogen bonding interaction with Ser264. Interestingly, its neighboring residue Ile263 is in close proximity to the Y• (Tyr177) and

may influence Y• stability (Figure 8). Docking of $\mathbf{H_2L^2}$ (GS = 48) showed a slightly altered pose within the binding pocket (Figure 7) but was also predicted to have the hydrophobic core situated deep in the pocket, and shared the hydrogen bonding interaction to Ser264. Similar docking results of the active compounds suggest plausible binding to R2 RNR. However, a crystal structure would give more comprehensive information about the interaction of $\mathbf{H_2L^2}$ and **3** with the R2 protein.

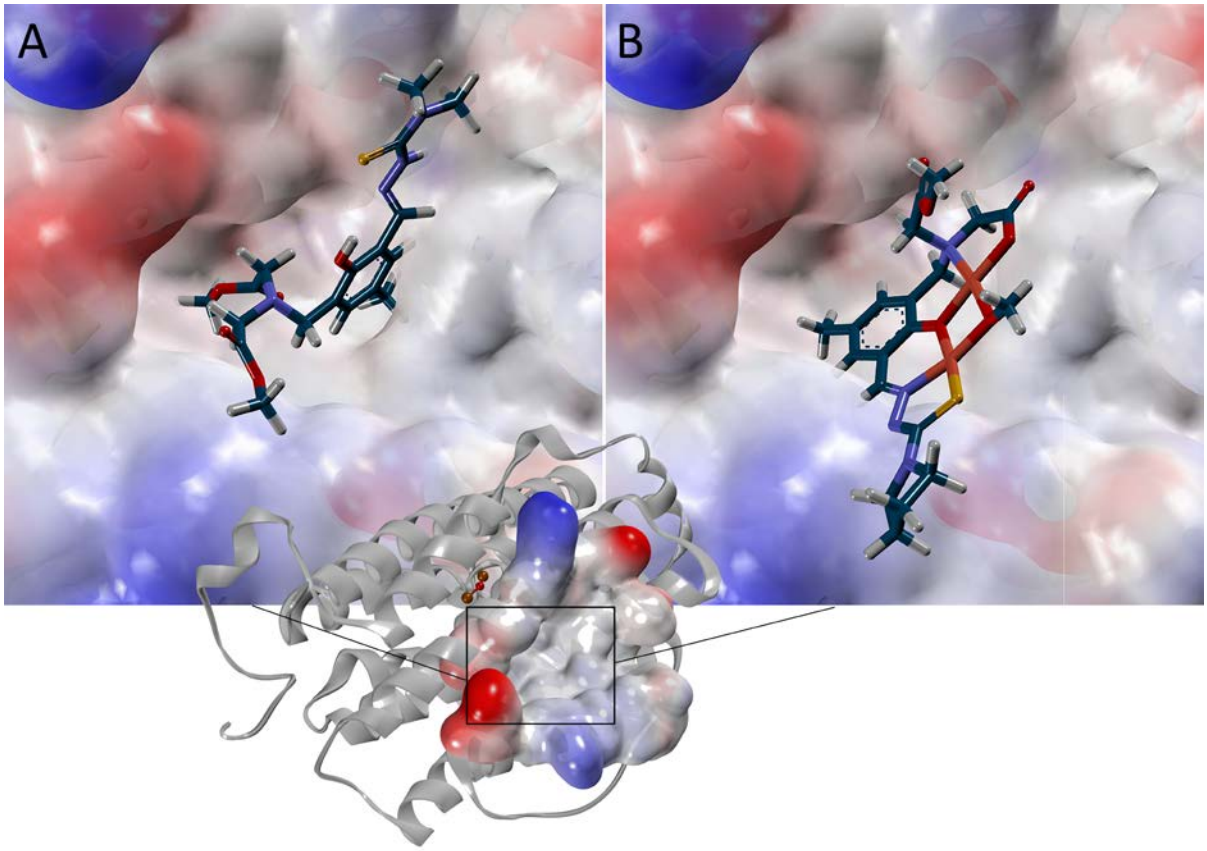

Figure 7. Binding site of RNR R2 (PDBid:1W68), showing the docked configuration of $\mathbf{H_2L^2}$ (A) and of complex **3** (B)**.** The protein surface is rendered, blue and red depict positive and negative charges, respectively.

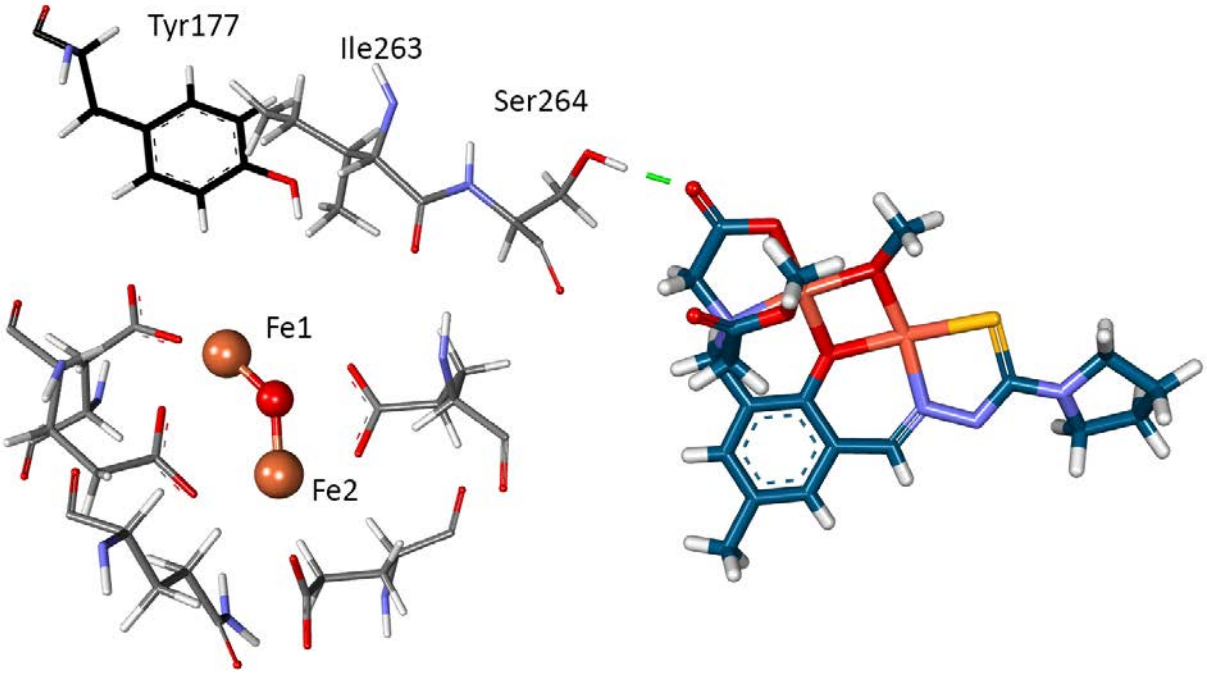

Figure 8. Predicted hydrogen bonding interaction between complex **3** and Ser264 in R2 (PDBid:1W68). An alteration to Ser264 conformation may lead to further conformational changes and modulate protein activity.

Interaction with Ribonucleotide Reductase – Binding Affinity Measurements. Biomolecular interaction analysis gives fundamental insights into the molecular biology of the cell, but is also an important pharmacological tool. Microscale Thermophoresis (MST) allows for quantitative analysis of protein interactions in solution, and is sensitive to all types of binding-induced changes of molecular properties, such as size, charge, solvation shell or conformation. The technique is based on thermophoresis, the directed motion of molecules in temperature gradients. Initially, an infrared laser is used for heating of the samples, and the movement of molecules in the temperature gradient can be analyzed via protein intrinsic UV-fluorescence. The intrinsic protein fluorescence upon interaction with the proligands or metal complexes arises from the aromatic amino acids, with tryptophan (Trp) being the dominant intrinsic fluorophore.[49] As a change in the fluorescence intensity was observed with increasing concentrations of both compounds, $\mathbf{H_2L^2}$ and **3**, the fluorescence quenching signal was used directly for affinity determination. From the binding affinity studies of both compounds tested against mouse R2 protein, we obtained K_D values in the low µM range, with K_Ds of 2.7 ± 0.4 µM and 3.3 ± 0.4 µM for $\mathbf{H_2L^2}$ and **3**, respectively (Figure 9). Regarding the proligand $\mathbf{H_2L^2}$, these values are in the same general range established by the enzymatic IC_{50} values for the proligand (also reported in this paper to be between 4.2 and 5.4 µM for HeLa, K562, A549 and LS-174 cell lines). Regarding the copper(II) complex **3**, however, although the K_D values are equivalent to those

obtained for $\mathbf{H_2L^2}$, the complex shows lower selectivity towards cancer cells. Interestingly, $\mathbf{H_2L^2}$ and **3** are predicted to have the same binding affinity in line with the affinity measurements. Despite these differences, both compounds show a significant effect on the Y• destruction in the mouse R2 protein, as seen from the kinetic monitoring of the Y• concentration by EPR (Figures 10 and 11). The structural nature of the binding interactions of the investigated compounds and R2 protein are not resolved from the MST assay, therefore, molecular modeling of the R2 protein and the compounds $\mathbf{H_2L^2}$ and **3**, was also performed in this study.

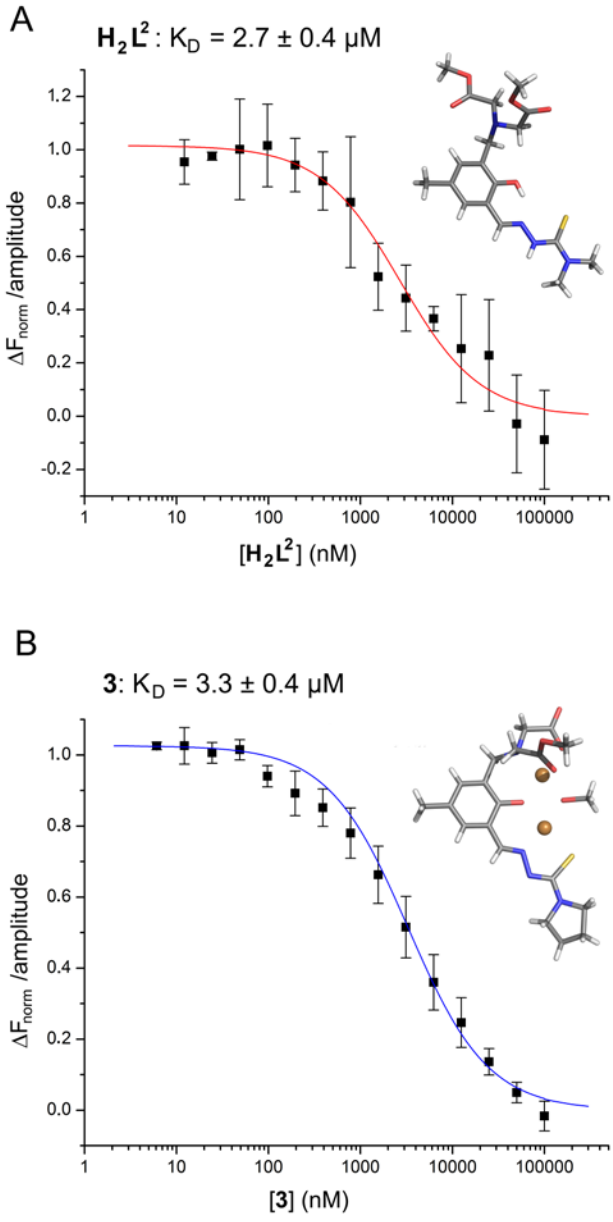

Figure 9. Binding curves for the interaction of $\mathbf{H_2L^2}$ (A) and **3** (B) with mouse R2. The changes in fluorescence signals were fitted (lines) to yield K_D values of 2.7 ± 0.4 µM and 3.3 ± 0.4 µM for $\mathbf{H_2L^2}$ and **3**, respectively.

Interaction with Ribonucleotide Reductase – Effect on Y•. The effect of the proligand $\mathbf{H_2L^2}$ and

complex **3** on the Y• in mouse R2 protein was tested by low-temperature EPR spectroscopy. X-band (9.4 GHz) absorption derivative spectra were recorded at 30 K. Highly purified iron-reconstituted R2 protein in buffer containing 1% DMSO was incubated with the two compounds, along with the control sample (blank) for 1 min at 298 K. For the first set of EPR measurements, 55 μM R2 monomer was incubated with 40 μM of each compound, whereas for the second set of EPR measurements, 50 μM protein was incubated with an equal concentration of compounds, yielding a 1:1 molar ratio. In the latter case, DTT was also added in two steps, where spectra recorded after 6.5 and 146 min incubation time correspond to sample incubations after addition of 0.5 and 1 mM dithiothreitol (DTT), respectively. Between each recording of spectra, samples were simultaneously thawed, incubated for the indicated times (see Table 3 for total times of incubation), and quickly refrozen in liquid nitrogen. As seen in Table 3 and Figures 10 and 11, the effect of $\mathbf{H_2L^2}$ and **3** on the Y• signal is clearly seen in both cases, indicating a faster destruction of the Y• as compared to the blank samples. Furthermore, the depletion of the signal is even more evident in the presence of DTT, where a distinct reduction of the signal is especially observed after the addition of 1 mM DTT, recorded after a total incubation time of 146 min at 298 K. In comparison, the Y• signal is slowly decreased at the equivalent incubation time in the blank sample. Previous studies have shown that 1% DMSO in the samples has no effect on the natural decay of Y•, and is not accounted for in this study.[50] The decay of the Y• is shown in Figures 10 and 11, for measurements in the presence and in the absence of DTT. As seen from the EPR experiments, $\mathbf{H_2L^2}$ shows the greatest effect on the Y•, as compared to **3**, resulting in the lowest Y• content after 1226 min total incubation time at room temperature. This is also observed from the UV–vis spectroscopy, where the peak at 408 nm, characteristic of a tyrosyl radical, was followed. The Y• seems to be quenched to a larger extent in the presence of $\mathbf{H_2L^2}$ than in the presence **3** (Figure 12). As both compounds bind to the R2 protein with low μM affinities, and show significant effects on Y• quenching, these results taken together strongly indicate that both $\mathbf{H_2L^2}$ and **3** serve as effective R2 inhibitors.

Table 3. Mouse R2 tyrosyl radical (Y•) content in reconstituted R2 protein and $\mathbf{H_2L^2}$ and **3**, after different incubation times at 298 K.

		Tyrosyl radical (Y•)					
		R2 (blank)		**R2 + H_2L^2**		**R2 + 3**	
	Time (min)	**Y•/R2**[†]	**%**[‡]	**Y•/R2**[†]	**%**[‡]	**Y•/R2**[†]	**%**[‡]
Run #1[§]	**1**	0.45	100	0.44	97.8	0.42	93.3
	16	0.41	91.1	0.39	86.7	0.38	84.8

	116	0.34	75.6	0.25	55.6	0.24	53.3
	446	0.17	37.8	0.14	31.1	0.14	31.1
	1450	0.09	20	0.03	6.7	0.05	11.1
Run #2[¶]	**1**	0.34	100	0.4	117.6	0.38	111.7
	6.5 (+ 0.5 mM DTT)	0.3	88.2	0.34	100	0.33	97
	26	0.29	85.3	0.3	88.2	0.34	100
	86	0.3	88.3	0.24	70.6	0.26	76.5
	146 (+ 1 mM DTT)	0.22	64.7	0.006	1.8	0.04	11.8
	1226	0.02	5.9	0	0	0.001	0.3

[†] Yield of tyrosyl radical (Y•)/R2 monomer
[‡] Percent compared to untreated R2 (blank) sample at time 1 min
[§] First set of EPR measurements (molar ratio of ~ 0.75 tested compound/R2 monomer)
[¶] Second set of EPR measurements, with addition of DTT (molar ratio of 1 tested compound/R2 monomer)

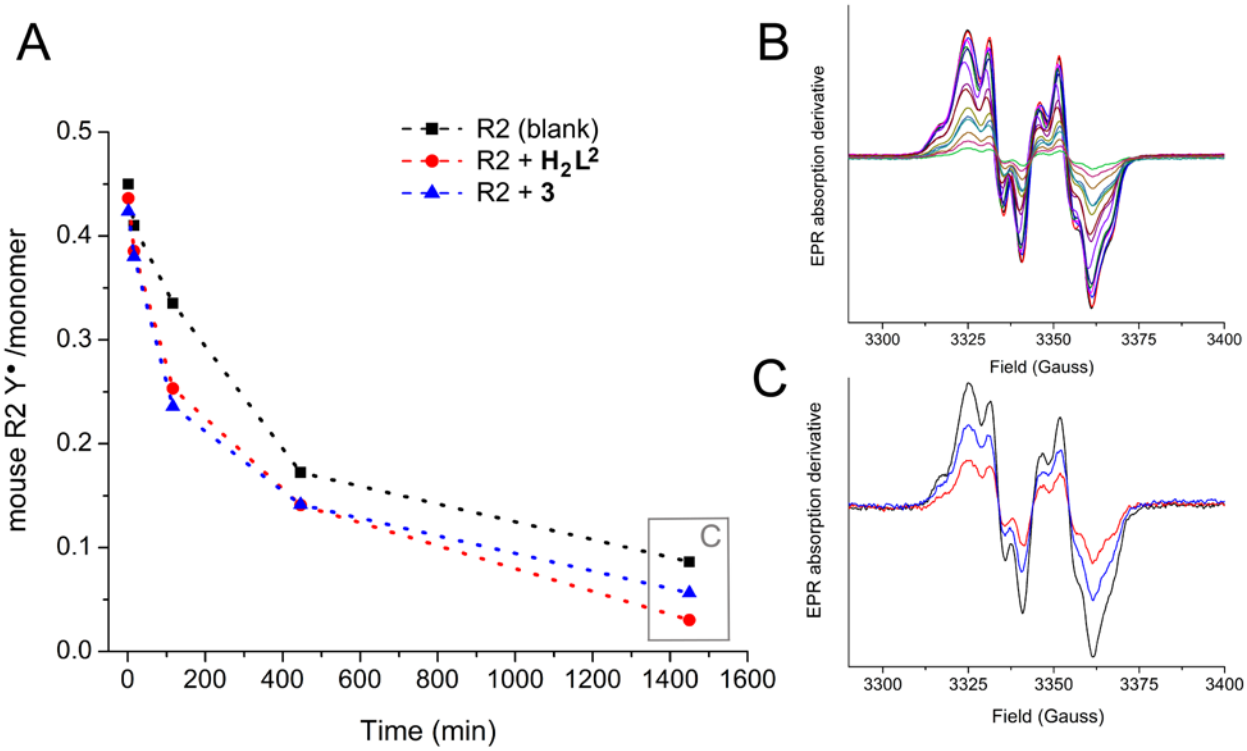

Figure 10. The effect of $\mathbf{H_2L^2}$ and **3** on mouse R2 tyrosyl radical (Y•) content. (A) Y• yield/R2 monomer in samples containing 55 µM R2 and 40 µM tested compound, measured after 1, 16, 116, 446, and 1450 min total incubation time at 298 K. (B) X-band EPR spectra showing decreasing Y• content following increasing incubation times at 298 K. (C) EPR spectra of R2 (black trace), R2 with $\mathbf{H_2L^2}$ (red trace), and R2 with **3** (blue trace), recorded after a total incubation time of 1450 min at 298 K. $\mathbf{H_2L^2}$ shows the largest effect on the quenching of Y•.

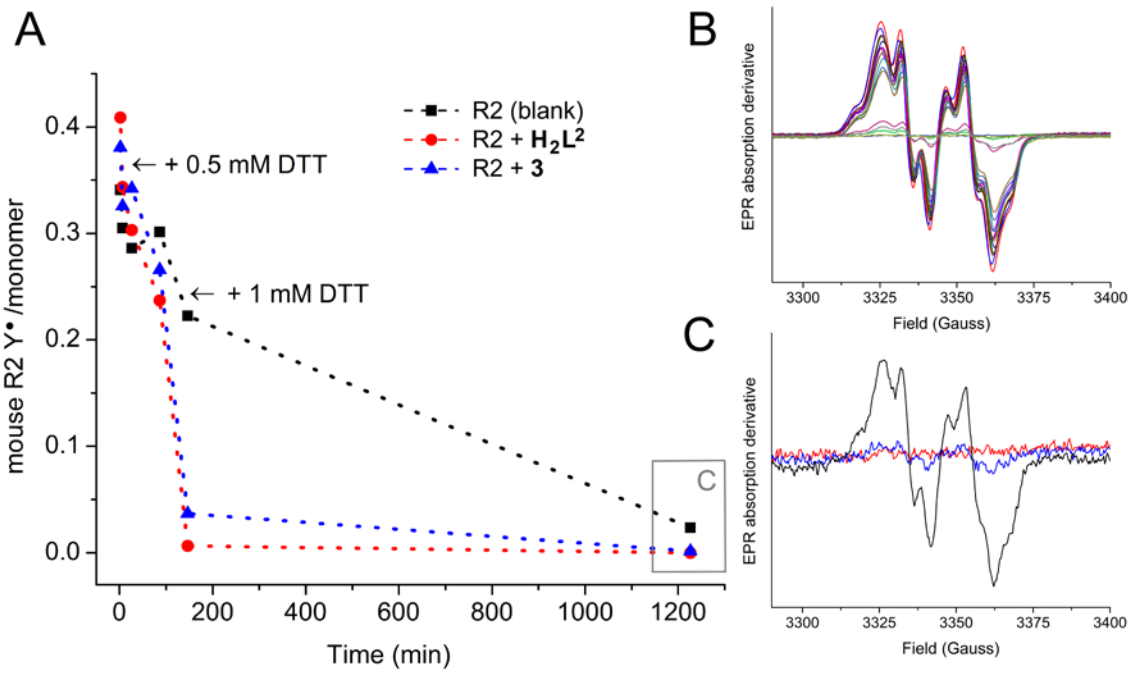

Figure 11. The effect of $\mathbf{H_2L^2}$ and **3** on mouse R2 tyrosyl radical (Y•) content in the presence of DTT. (A) Y• yield/R2 monomer in samples containing 50 µM R2 and 50 µM tested compound, measured after 1, 6.5, 26, 86, 146, and 1226 min total incubation time at 298 K. 0.5 mM DTT and 1 mM DTT was added to the samples prior to incubation at 298 K for 6.5 min and 146 min in total, respectively. (B) X-band EPR spectra showing decreasing Y• content following increasing incubation times at 298 K. A substantial loss of the Y• content is observed after the addition of 1 mM DTT in samples containing both compounds. (C) EPR spectra of R2 (black trace), R2 with $\mathbf{H_2L^2}$ (red trace), and R2 with **3** (blue trace), containing a total concentration of 1.5 mM DTT, recorded after a total incubation time of 1226 min at 298 K. $\mathbf{H_2L^2}$ shows the largest effect on the quenching Y•, as seen for EPR experiments without the addition of DTT. However, the effect of **3** is in this case greater than observed in R2 samples where DTT was not added (see Figure 10 and Table 2).

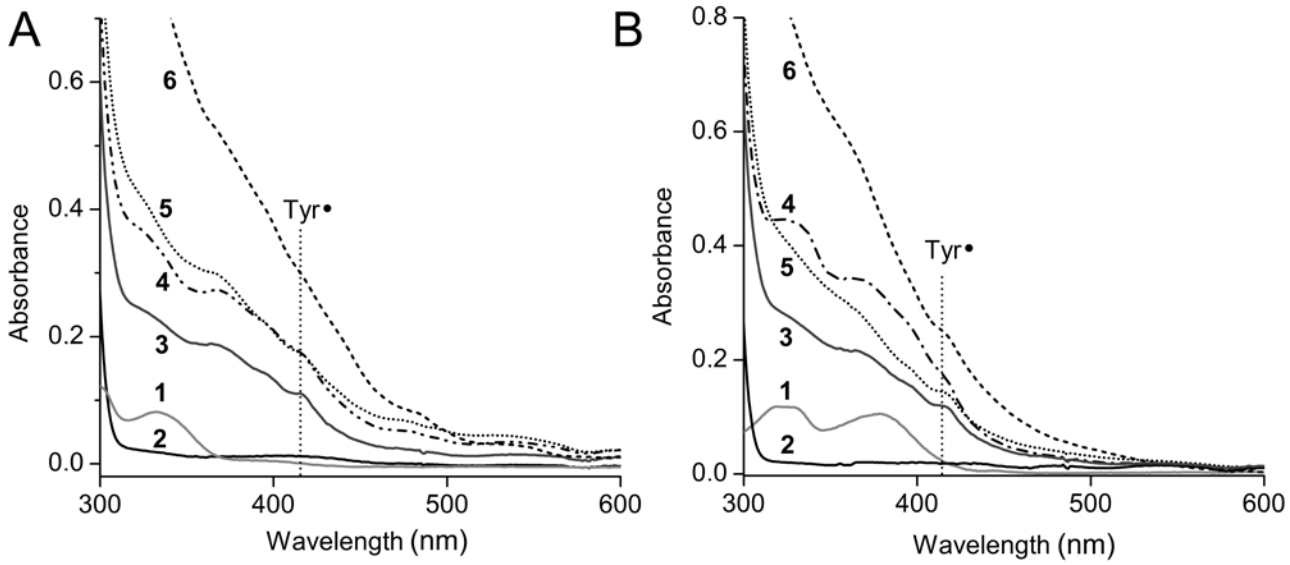

Figure 12. UV–vis spectra of mouse R2 with $\mathbf{H_2L^2}$ (A) and **3** (B). In both (A) and (B), the different spectra represent the following: **1**) 6 µM compound; **2**) 30 µM apo-R2; **3**) 30 µM reconstituted R2 (R2-Fe(III)$_2$-Y•); **4**) as **3** + 6 µM compound (10 min incubation); **5**) as **4** + 1 mM DTT (5 min incubation); **6**) as **5** + 24 µM compound + 1 mM DTT (10 min incubation).

Conclusions

A series of six iminodiacetate-thiosemicarbazone hybrids and six dicopper(II) complexes, the latter resulting from reactions of copper(II) salts with the proligands, have been synthesized and characterized by X-ray diffraction, analytical and spectroscopic techniques. All compounds were assayed for antiproliferative activity in four cancer and one noncancerous cell lines showing moderate to high cytotoxicity often exceeding that of the clinical drug cisplatin. There are no clear-cut structure–activity relationships to be mentioned. The effect of copper(II) coordination is manifested in a divergent way. In some cases, as for $\mathbf{H_2L^1}$, binding of copper(II) results in a 2- to 10-fold enhancement of antiproliferative activity, while in the case of $\mathbf{H_2L^3}$, a 2- to 14-fold decrease of activity is observed in cancer cell lines. In addition, $\mathbf{H_2L^4}$ and $\mathbf{H_2L^5}$ underwent chemical transformations induced by copper(II) coordination, resulting in formation of new ligands $(HL^4)^-$ and $(HL^5)^-$. Therefore, the proligands $\mathbf{H_2L^4}$ and $\mathbf{H_2L^5}$ and their corresponding copper(II) complexes are not directly comparable. It is also worth mentioning the effect of thiomethylation of the thiosemicarbazide moiety on cytotoxicity, which is divergent for organic hybrids and dicopper(II) complexes. Compound **6** is by a factor of 2 in average less active than **1**, while $\mathbf{H_2L^6}$ is generally more cytotoxic than $\mathbf{H_2L^1}$ in cancer cell lines. The selectivity of $\mathbf{H_2L^2}$ and **3** for cancer vs noncancerous cells deserves to be mentioned as well. Taking into account the observed selectivity for cancer cells, both these compounds and for comparison reasons, complex **2** and proligand $\mathbf{H_2L^3}$ were chosen for further studies into the mechanism of antiproliferative activity, and for interaction studies with the R2 protein of RNR. The absence of early and late apoptotic populations established by flow cytometry dual staining of K562 cells with annexin V-FITC and PI and cell cycle analysis indicated that other mechanisms of antiproliferative activity are involved in the case of complex **2**. The likelihood of binding of $\mathbf{H_2L^2}$ and **3** to mouse R2 RNR was suggested by molecular docking calculations. Binding affinity measurements performed by microscale thermophoresis afforded K_D values in the low μM range indicating formation of adducts and possible inhibition of RNR. Indeed, both compounds showed a marked effect on destruction of the tyrosyl radical in mouse R2 protein monitored by kinetic measurements of the Y• concentration by EPR and UV–vis spectroscopies. The effect was more pronounced in the presence of DTT, as seen from EPR measurements. The compounds investigated in this work deserve further investigation into the mechanisms of antiproliferative and R2 inhibition activities as potential anticancer drugs.

Experimental Section

Materials. Dimethyliminodiacetate hydrochloride (Alfa Aesar), sodium hydrogen carbonate (Alfa Aesar), thiosemicarbazide (Alfa Aesar), 4,4'-dimethyl-thiosemicarbazide (Alfa Aesar), (trimethylsilyl)methylamine (Aldrich), copper(II) chloride dihydrate and copper(II) acetate monohydrate were used as received. Tetrahydrofuran (THF), dichloromethane (DCM), chloroform, diethylether, ethanol and methanol were received from Acros. 4-*N*-pyrrolidine-thiosemicarbazide, S-methylisothiosemicarbazide hydroiodide, 4-(1-naphthyl)-3-thiosemicarbazide and S-methyl-hydrazinecarbodithioate were synthesized by following literature procedures.[51] 3-(Chloromethyl)-2-hydroxy-5-methylbenzaldehyde (A) was prepared from 5-methyl-2-hydroxy-benzaldehyde according to a procedure reported elsewhere.[33]

(Trimethylsilyl)methyl thiosemicarbazide has been prepared by reacting S-methylhydrazinecarbodithioate (2.00 g, 16.5 mmol) with (trimethylsilyl)methylamine (2 mL, 15 mmol) in ethanol (40 mL) at reflux overnight, followed by chromatographic separation using chloroform as eluent. Yield: 1.34 g, 52%. ^{1}H NMR (DMSO-d_6, δ_H, ppm): 8.49 (s, 1H, NH), 7.58 (s, 1H, NH), 4.46 (s, 2H, NH_2), 3.04 (d, J = 5.7 Hz, 2H, CH_2), 0.06 (s, 9H, CH_3). ESI-MS (methanol): positive *m/z* 178 $[M + H]^+$. ATR-IR, cm^{-1} : 3261m, 3242m, 2955w, 2897w, 1553s, 1502m, 1478w, 1414m, 1373w, 1288m, 1250s, 1202m, 1055m, 922w, 843vs, 764m, 696m, 640s, 592m.

Synthesis of proligands

Dimethyl-2,2'-((3-formyl-2-hydroxy-5-methylbenzyl)-azanediyl)diacetate (B). To a solution of dimethyliminodiacetate hydrochloride (1.00 g, 5.00 mmol) in DCM (25 mL) a solution of 3-(chloromethyl)-2-hydroxy-5-methylbenzaldehyde (**A**) (0.90 g, 5.00 mmol) in THF (25 mL) and triethylamine (3 mL) were added. The color changed to yellow. The reaction mixture was stirred at room temperature overnight. The precipitate formed was filtered off. The filtrate was concentrated under reduced pressure to afford yellow oil, which was dissolved in DCM (30 mL) and poured into a saturated aqueous solution of sodium hydrogen carbonate (75 mL). The organic layer was separated and the aqueous solution was extracted with DCM (2 × 10 mL). The combined organic extracts were concentrated under reduced pressure to give yellow oil which was dried *in vacuo*. Yield: 1.3 g, 83%. ^{1}H NMR (400.10 MHz, $CDCl_3$, δ, ppm): 10.66 (s, 1H, -OH), 10.16 (s, 1H, CH=O), 7.41 (s, 1H, Ar H), 7.34 (s, 1H, Ar H), 3.99 (s, 2H, CH_2), 3.74 (s, 6H, CH_3), 3.60 (s, 4H, CH_2), 2.32 (s, 3H, CH_3). ESI–MS (methanol): positive *m/z* 310 $[M + H]^+$, 332 $[M + Na]^+$. ATR–IR, cm^{-1}: 3290vw, 2945m,

2745vw, 2602m, 1740vs, 1647s, 1607m, 1470s, 1443s, 1393m, 126s, 1205vs, 1155s, 1022s, 1005s, 872m, 800m, 727m, 633m, 554w.

H_2L^1. To a solution of the aldehyde **B** (0.31 g, 1.00 mmol) in methanol (5 mL) a hot solution of thiosemicarbazide (0.09 g, 1.00 mmol) in water (5 mL) was added. The mixture was stirred to reflux for 1 h and a yellow precipitate was formed. The solid was filtered off, washed with cold methanol/water 1:1 (3 × 5 mL), then with cold methanol (3 mL) and diethylether (3 mL) and dried *in vacuo*. Single crystals of X-ray diffraction quality were obtained by recrystallization of the raw product from methanol/chloroform 1:1. Yield: 0.35 g, 93%. Anal. Calcd for $C_{16}H_{22}N_4O_5S$ (M_r 382.43): C, 50.25; H, 5.80; N, 14.65; S, 8.38. Found: C, 50.70; H, 5.80; N, 14.55; S, 8.12. ^{1}H NMR 400.13 MHz (DMSO-d_6, δ, ppm): 11.42 (s, 1H, NH), 9.76 (s, 1H, OH), 8.38 (s, 1H, H7), 8.12 (s, 1H, NH), 7.93 (s, 1H, NH), 7.75 (s, 1H, H5), 6.91 (s, 1H, H3), 3.86 (s, 2H, H10), 3.66 (s, 6H, H13), 3.54 (s, 4H, H11), 2.21 (s, 3H, H9). ^{13}C NMR 100.6 MHz (DMSO-d_6, δ, ppm): 177.6 (C8), 171.1 (C12), 153.7 (C1), 139.2 (C7), 132.0 (C3), 127.7 (C4), 126.0 (C5), 122.5 (C2), 120.2 (C6), 54.8 (C10), 53.3 (C11), 51.6 (C13), 19.9 (C9). ESI–MS (methanol), positive *m/z* 383 $[M + H]^+$, 405 $[M + Na]^+$. UV–vis (methanol), λ_{max} (ε, $M^{-1}cm^{-1}$): 224_{sh}, 301 (17500), 310 (18033), 339 (19432), 392_{sh} at 2.4 × 10^{-5} M. ATR–IR, cm^{-1}: 3448m, 3335m, 3165w, 3026w, 2953w, 2916w, 1730vs, 1595m, 1535s, 1452m, 1379m, 1286s, 1203vs, 1155s, 1103s, 1065w, 1013m, 957s, 905w, 868w, 835m, 733m, 642m, 625m, 588w.

H_2L^2. To a solution of **B** (0.31 g, 1.00 mmol) in methanol (5 mL) a hot solution of 4,4'-dimethyl-thiosemicarbazide (0.12 g, 1.00 mmol) in water (5 mL) was added. The mixture was stirred at reflux for 1 h. Yellow crystals of X-ray diffraction quality were obtained when the mixture has cooled to room temperature. The crystals were filtered off, washed with water (3 x 5 mL) and dried in air at room temperature. Yield: 0.32 g, 88%. Anal. Calcd for $C_{18}H_{26}N_4O_5S{\cdot}0.5\ H_2O$ (M_r 419.49): C, 51.54; H, 6.49; N, 13.36; S, 7.64. Found: C, 51.24; H, 6.47; N, 13.34; S, 7.57. ^{1}H NMR 400.13 MHz (DMSO-d_6, δ, ppm): 11.73 (s, 1H, OH), 11.22 (s, 1H, NH), 8.47 (s, 1H, H7), 7.19 (d, *J* = 1.6 Hz, 1H, H3), 7.09 (d, *J* = 2.0 Hz, 1H, H5), 3.86 (s, 2H, H10), 3.62 (s, 6H, H13), 3.54 (s, 4H, H11), 3.30 (s, 6H, H17, 18), 2.25 (s, 3H, H9).^{13}C NMR 100.6 MHz (DMSO-d_6, δ, ppm): 179.1 (C8), 171.2 (C12), 153.3 (C1), 146.5 (C7), 132.2 (C3), 129.1 (C5), 127.0 (C4), 124.9 (C2), 117.7 (C6), 53.8 (C11), 51.1 (C13), 50.9 (C10), 41.0 (C17, C18), 20.0 (C9). ESI–MS (methanol), positive: *m/z* 433 $[M + Na]^+$. UV–vis (methanol), λ_{max} (ε, $M^{-1}cm^{-1}$): 226 (29002), 288 (26124), 302_{sh}, 338 (19709), 397 (1993) at 1.8 × 10^{-5} M. ATR–IR, cm^{-1}: 3445vw, 3306m, 2999vw, 2951w, 2924w, 2856w, 1724vs, 1616w,

1547s, 1502w, 1450m, 1420m, 1379m, 1346m, 1321s, 1292s, 1254s, 1213vs, 1171m, 1148s, 1117s, 1061w, 1040w, 1001s, 976w, 951m, 910m, 889w, 870m, 845m, 789s, 756m, 719w, 689m, 652w.

H_2L^3. To a solution of **B** (0.31 g, 1.00 mmol) in methanol (5 mL) a hot solution of 4*N*-pyrrolidine-thiosemicarbazide (0.15 g, 1.00 mmol) in methanol/water 1:2 (15 mL) was added. The resulting mixture was stirred at reflux for 1 h and a yellow precipitate was formed. The solid was filtered off, washed with cold methanol/water 1:1 (3 × 5 mL), then with cold methanol (3 mL) and diethylether (3 mL) and dried *in vacuo*. Single crystals of X-ray diffraction quality were obtained by recrystallization of the raw product from methanol. Yield: 0.40 g, 91%. Anal. Calcd for $C_{20}H_{28}N_4O_5S$ (M_r 436.52): C, 55.03, H, 6.46, N, 12.83, S, 7.35. Found: C, 54.80, H, 6.43, N, 12.50, S, 7.08. ^{1}H NMR 400.13 MHz (DMSO-d_6, δ, ppm): 11.56 (s, 1H, OH), 10.98 (s, 1H, NH), 8.45 (s, 1H, H7), 7.18 (d, *J* = 1.2 Hz, 1H, H3), 7.08 (d, *J* = 1.6 Hz, 1H, H5), 3.88 (s, 2H, H10), 3.68 (t, *J* = 6.4 Hz, 4H, H17, H20), 3.63 (s, 6H, H13), 3.54 (s, 4H, H11), 2.26 (s, 3H, H9), 1.95 (t, *J* = 6.4 Hz, 4H, H18a, H19a). ^{13}C NMR 100.6 MHz (DMSO-d_6, δ, ppm): 175.9 (C8), 170.8 (C12), 153.1 (C1), 145.7 (C7), 131.8 (C3), 128.6 (C5), 126.8 (C4), 124.7 (C2), 117.7 (C6), 53.8 (C11), 51.2 (C10), 50.8 (C13), 50.1 (C17, C20), 24.4 (C18a, C19a), 19.7 (C9). ESI–MS (methanol), positive *m/z* 459 $[M + Na]^+$. UV–vis (methanol), λ_{max} (ε, $M^{-1}cm^{-1}$): 206 (28864), 225 (27477), 288 (21620), 336 (14430), 394_{sh} at 2.1×10^{-5} M. ATR–IR, cm^{-1}: 3290m, 3084vw, 2947w, 2862w, 1726vs, 1651vw, 1616w, 1551s, 1460s, 1421s, 1358m, 1340s, 1296vs, 1246m, 1215vs, 1190vs, 1157s, 1128s, 1038m, 999s, 941m, 908m, 868m, 785m, 752m, 710m, 675m, 646m, 575w.

H_2L^4. To a solution of **B** (0.31 g, 1.00 mmol) in methanol (5 mL) a solution of (trimethylsilyl)methylthiosemicarbazide (0.17 g, 1.00 mmol) in water/methanol mixture 2:1 (15 mL) was added and the mixture was stirred at reflux for 1 h. The yellow precipitate was filtered off, washed with cold methanol/water 1:1 (3 × 5 mL), then with cold methanol (3 mL) and diethylether (3 mL) and dried in vacuo. Single crystals were obtained by recrystallization of the raw product from methanol/diethylether 1:2. Yield: 0.36 g, 77%. Anal. Calcd for $C_{20}H_{32}N_4O_5SSi$ (M_r 468.64): C, 51.26; H, 6.88; N, 11.96; S, 6.84. Found: C, 51.41; H, 6.88; N, 11.70; S, 6.67. ^{1}H NMR 500.13 MHz (DMSO-d_6, δ, ppm): 11.34 (s, 1H, NH), 9.80 (s, 1H, OH), 8.36 (s, 1H, H7), 8.19 (t, *J* = 6.0 Hz, 1H, NH), 7.59 (s, 1H, H5), 6.93 (s, 1H, H3), 3.87 (s, 2H, H10), 3.65(s, 6H, H13), 3.54 (s, 4H, H11), 3.21 (d, *J* = 6.0 Hz, 2H, H17), 2.22 (s, 3H, H9), 0.11 (s, 9H, H18-H20). ^{13}C NMR 125.7 MHz (DMSO-d_6, δ, ppm): 176.3 (C8), 171.2 (C12), 153.5 (C1), 138.7 (C7), 131.9 (C3), 127.6 (C4), 125.8 (C5), 122.7 (C2), 120.3 (C6), 54.6 (C10), 53.3 (C11), 51.6 (C13), 34.2 (C17), 20.1 (C9), –1.8 (C18-C20).

ESI–MS (methanol), positive *m/z* 491 $[M + Na]^+$. UV–vis (methanol), λ_{max} (ε, $M^{-1}cm^{-1}$): 235 (3184), 300 (18694), 313 (21691), 342 (33059), 355_{sh}, 398_{sh} at 2.3×10^{-5} M. ATR–IR, cm^{-1}: 3325w, 2955w, 1732s, 1607w, 1529s, 1480w, 1429m, 1329w, 1294s, 1246s, 1211s, 1184s, 1156m, 1111s, 1072m, 1013m, 953m, 895w, 847vs, 758m, 700m, 650m, 582m.

H_2L^5. To a solution of **B** (0.31 g, 1.00 mmol) in methanol (5 mL) a solution of 4-(1-naphthyl)-3-thiosemicarbazide (0.21 g, 1.00 mmol) in methanol/water 1:2 (15 mL) was added. The resulting mixture was stirred at reflux for 1 h and a yellow precipitate was formed. The product was filtered off, washed with cold methanol/water 1:1 (3 × 5 mL), then with cold methanol (3 mL) and diethylether (3 mL) and dried in vacuo. Single crystals were obtained by recrystallization of the raw product from acetonitrile/chloroform 1:1. Yield: 0.42 g, 84%. Anal. Calcd for $C_{26}H_{28}N_4O_5S \cdot 0.3H_2O$ (M_r 513.99): C, 60.76, H, 5.61, N, 10.90, S, 6.24. Found: C, 61.10, H, 5.51, N, 10.54, S, 5.91. ^{1}H NMR 400.13 MHz (DMSO-d_6, δ, ppm): 11.93 (s, 1H, NH), 10.32 (s, 1H, NH), 9.83 (s, 1H, OH), 8.57 (s, 1H, H7), 8.01–7.52 (m, 8H, H5, H18-25), 6.93 (s, 1H, H3), 3.89 (s, 2H, H10), 3.67 (s, 6H, H13), 3.57 (s, 4H, H11), 2.20 (s, 3H, H9). ^{13}C NMR 100.6 MHz (DMSO-d_6, δ, ppm): 177.6 (C8), 171.2 (C12), 153.8 (C1), 139.6 (C7), 133.7 (C3), 126.4 (C5), 135.8, 132.2, 130.7, 127.9, 127.7, 126.9, 126.0, 125.4, 123.4 (C4, C18-C25), 122.5 (C2), 120.3 (C6), 54.9 (C10), 53.3 (C11), 51.6 (C13), 20.0 (C9). ESI–MS (methanol), positive *m/z* 531 $[M + Na]^+$. UV–vis (methanol), λ_{max} (ε, $M^{-1}cm^{-1}$): 221 (44904), 305 (16000), 314 (16570), 344 (21186) at 2×10^{-5} M. ATR–IR, cm^{-1}: 3331w, 3209m, 3045w, 3013w, 2955, 2885w, 2956w, 1720s, 1597w, 1531s, 1487s, 1431s, 1373m, 1288s, 1211vs, 1088m, 999s, 957m, 868m, 768m, 731m, 679m, 633m, 600w, 573vw.

H_2L^6. To a solution of **B** (0.64 g, 2.00 mmol) in methanol (5 mL) a solution of S-methyl-isothiosemicarbazide hydroiodide (0.47 g, 2.0 mmol) in methanol/water 1:2 (15 mL) was added. The resulting mixture was stirred at reflux for 1 h, then a solution of sodium hydrogen carbonate (0.17 g, 2.0 mmol) in water (5 mL) was added. A yellow oil was formed which was decanted, washed with cold methanol/water 1:1 (3 mL), dissolved in DCM (10 mL) and extracted with water (3 × 30 mL). The organic layer was concentrated under reduced pressure and dried in vacuo to afford yellow oil. Single crystals of X-ray diffraction quality were obtained by recrystallization of the raw product from methanol/water 1:1. Yield: 0.63 g, 76%. Anal. Calcd for $C_{17}H_{24}N_4O_5S \cdot 0.2MeOH$ (M_r 402.87): C, 51.28; H, 6.20; N, 13.91; S, 7.96. Found: C, 51.51; H, 6.23; N, 13.56; S, 7.60. ^{1}H NMR 400.13 MHz (DMSO-d_6, δ, ppm): 9.63 (s, 2H, NH2), 8.68 (s, 1H, H7), 7.82 (s, 1H, H5), 7.05 (s, 1H, H3), 3.94 (s, 2H, H10), 3.63 (s, 6H, H13), 3.60 (s, 4H, H11), 2.71 (s, 3H, H17), 2.21 (s, 3H, H9). ^{13}C

NMR 100.6 MHz (DMSO-d_6, δ, ppm): 171.0 (C12), 166.1 (C8), 155.2 (C1), 149.2 (C7), 135.0 (C3), 128.8 (C4), 127.5 (C5), 122.6 (C2), 119.2 (C6), 55.3 (C10), 53.8 (C11), 52.2 (C13), 20.2 (C9), 13.7 (C17). ESI–MS (methanol), positive *m/z* 419 $[M + Na]^+$, 815 $[2{\cdot}M + Na]^+$. UV–vis (methanol), λ_{max} (ε, $M^{-1}cm^{-1}$): 226 (3777), 298 (21292), 311 (22983), 341 (26666), 353 (23807) at 1.3×10^{-5} M. ATR–IR, cm^{-1}: 3456w, 3344w, 3124vw, 2999, 2951w, 2864, 1736vs, 1610s, 1524vs, 1460s, 1437s, 1377m, 1337m, 1288s, 1252s, 1202vs, 1153vs, 1007s, 973s, 864m, 744m, 667w, 629w, 577w.

Synthesis of copper(II) complexes

$[Cu(HL^1)Cl_3]{\cdot}2H_2O$ ($1{\cdot}2H_2O$). To a suspension of **H_2L^1** (0.19 g, 0.5 mmol) in methanol (10 mL) a solution of copper(II) chloride dihydrate (0.17 g, 1 mmol) in methanol (5 mL) was added. The color changed to dark brown. The mixture was stirred at 60 °C for 1 h, then cooled to room temperature and left for crystallization at room temperature. X-ray diffraction-quality single crystals were obtained after 48 h, washed with cold methanol and dried in air at room temperature. Yield: 0.15 g, 45%. Anal. Calcd for $C_{16}H_{21}Cl_3Cu_2N_4O_5S{\cdot}2H_2O$ (M_r 650.97), %: C, 29.52; H, 3.87; N, 8.61; S, 4.90. Found, %: C, 29.73; H, 3.66; N, 8.32; S, 4.84. Solubility in water: ≥ 8.00 mg/mL. ESI–MS (methanol), positive *m/z* 543 $[Cu^{II}_2(L^1)Cl]^+$, 480 $[Cu^{II}(HL^1)Cl + H]^+$, 444 $[Cu^{II}(L^1) + H]^+$. UV–vis (methanol), λ_{max} (ε, $M^{-1}cm^{-1}$): 202 (26316), 234 (18471), 276 (13604), 319 (14583), 374 (12527) at 1.1×10^{-5} M, 660 (191) at 1.3×10^{-3} M. ATR–IR, cm^{-1}: 3564w, 3394vw, 3269m, 3117w, 2953w, 2918w, 1713vs, 1649s, 1618s, 1566vs, 1460s, 1433s, 1366m, 1344m, 1271m, 1238s, 1215s, 1169s, 1101m, 1068m, 1029, 968s, 901m, 858s, 814s, 777m, 731m, 640m, 590s.

$[Cu_2(L^2)(OMe)]$ (2). To a suspension of **H_2L^2** (0.20 g, 0.5 mmol) in methanol (10 mL) a suspension of copper(II) acetate monohydrate (0.20 g, 1.0 mmol) in methanol (10 mL) was added. The color changed to dark brown. The mixture was stirred at room temperature for 1 h, then filtered and allowed to stand at room temperature. X-ray diffraction-quality single crystals were filtered off after 48 h, washed with cold methanol and dried in air at room temperature. Yield: 0.14 g, 25%. Anal. Calcd for $C_{18}H_{24}Cu_2N_4O_6S$ (M_r 551.56): C, 39.20, H, 4.39, N, 10.16, S, 5.81 Found: C, 39.20, H, 4.47, N, 9.85 S, 5.65. ESI–MS (methanol), positive *m/z* 573 $[Cu_2(L^2)(OMe) + Na]^+$, 1125 $[\{Cu_2(L^2)(OMe)\}_2 + Na]^+$. UV–vis (methanol), λ_{max} (ε, $M^{-1}cm^{-1}$): 204 (54190), 237 (29115), 280 (15265), 324 (26840), 337 (27366), 376 (28198), at 1.2×10^{-5} M, 638 (145) at 1.5 x 10^{-3} M. ATR–IR, cm^{-1}: 2930w, 2808w, 1720m, 1664s, 1639s, 1591w, 1562m, 1510s, 1462m, 1414s, 1380m, 1342m, 1300w, 1265m, 1230m, 1202m, 1182w, 1131m, 1107w, 1078m, 1022s, 955m, 914m, 868m, 822m, 764m, 731s, 648s, 611vs, 581vs.

[$Cu_2(L^3)(OMe)$] (3). To a suspension of **H_2L^3** (0.26 g, 0.6 mmol) in methanol (10 mL) a suspension of copper(II) acetate monohydrate (0.23 g, 1.20 mmol) in methanol (10 mL) was added. The color changed to dark brown. The mixture was stirred at room temperature for 1 h, then filtered and allowed to stand at room temperature. X-ray diffraction-quality single crystals were filtered off after 72 h, washed with methanol and dried in air at room temperature. Yield: 0.14 g, 41%. Anal. Calcd for $C_{20}H_{27}Cu_2N_4O_6S$ (M_r 578.61): C, 41.52, H, 4.70, N, 9.68, S, 5.54 Found: C, 41.54, H, 4.61, N, 9.57 S, 5.48. ESI–MS (methanol), positive *m/z* 577 $[Cu_2(L^3)(OMe) + H]^+$, 599 $[Cu_2(L^3)(OMe) + Na]^+$, 1177 $[\{Cu_2(L^3)(OMe)\}_2 + Na]^+$. UV–vis (methanol), λ_{max} (ε, $M^{-1}cm^{-1}$): 200 (31051), 238 (23933), 279 (13447), 323 (19608), 335 (19502), 375 (19799) at 0.9×10^{-5} M, 638 (145) at 1.4×10^{-3} M. ATR–IR, cm^{-1}: 2966w, 2918w, 2868w, 2812w, 1726s, 1659s, 1593m, 1564m, 1487s, 1448vs, 1394m, 1329s, 1273s, 1217s, 1184m, 1107w, 1078m, 1032s, 1007s, 962m, 906s, 862m, 822s, 710s, 685m, 646s, 613s, 579s.

[$Cu_2(HL^4)Cl_3$] (4). To a solution of **H_2L^4** (0.117 g, 0.25 mmol) in methanol (5 mL) a solution of copper(II) chloride dihydrate (0.085 g, 0.5 mmol) in methanol (3 mL) was added. The resulting mixture was stirred at 50 °C overnight, then was allowed to evaporate at room temperature. X-ray diffraction-quality single crystals were filtered off after 48 h, washed with methanol and dried in air at room temperature. Yield: 0.10 g, 63%. Anal. Calcd for $C_{18}H_{25}Cl_3Cu_2N_4O_6S$ (M_r 658.93): C, 32.81, H, 3.82, N, 8.50, S, 4.87. Found: C, 32.82 , H, 3.97, N, 8.24, S, 4.78. Solubility in water: ≥ 8.00 mg/mL. ESI–MS (methanol), positive *m/z* 587 $[Cu^{II}_2(L^4)Cl]^+$, 488 $[Cu^{II}(HL^4)]^+$. UV–vis (methanol), λ_{max} (ε, $M^{-1}cm^{-1}$): 222 (13564), 234 (13321), 285 (14254), 314 (13342) 380 (11554) at 4.2×10^{-5} M, 634 (178) at 2.5×10^{-3} M. ATR–IR, cm^{-1}: 3180m, 3123w, 3026m, 2968w, 2935w, 2820vw, 1720s, 1612w, 1570vs, 1535s, 1456m, 1431s, 1360s, 1319s, 1276s, 1221vs, 1074vs, 962s, 908m, 860, 812m, 795m, 694s, 594m.

[$Cu_2(HL^5)Cl_3$] (5). To a suspension of **H_2L^5** (0.51 g, 1.00 mmol) in methanol (10 mL) a solution of copper(II) chloride dihydrate (0.17 g, 1.00 mmol) in methanol (5 mL) was added. The color changed to dark brown. The mixture was stirred at 60 ^oC for 1 h, then cooled to room temperature and left for crystallization at room temperature. X-ray diffraction-quality single crystals were filtered off after 48 h, washed with methanol and dried in air at room temperature. Yield: 0.15 g, 22%. Anal. Calcd for $C_{26}H_{25}Cl_3Cu_2N_4O_5S$ (M_r 739.02): C, 42.26 H, 3.41, N, 7.58, S, 4.34 Found: C, 42.18, H, 3.76, N, 7.28 S, 4.13. UV–vis (methanol), λ_{max} (ε, $M^{-1}cm^{-1}$): 227 (17591), 258 (11735), 346 (4415), 417

(6893) at 1.8×10^{-5} M, 696 (104) at 1.7×10^{-3} M. ATR–IR, cm^{-1}: 3223m, 3078, 3020vw, 2949w, 2916vs, 1720, 1614w, 1547s, 148s1, 1443s, 1377s, 1290s, 1248vs, 1229s, 1121s, 1095m, 1032m, 1005m, 955m, 897w, 860s, 80s0, 775m, 735m, 671m, 617m, 565vw.

$[Cu_2(L^6)Cl_3]\cdot 0.5H_2O$ (6·0.5H_2O). To a solution of **H_2L^6** (0.49 g, 1.2 mmol) in methanol (10 mL) a solution of copper(II) chloride dihydrate (0.31 g, 1.8 mmol) in methanol (5 mL) was added. The color changed to dark brown. The mixture was heated at 60 °C for 1 h and allowed to stand at room temperature for crystallization. The crystals were filtered off after 24 h, washed with methanol and dried in air at room temperature. Yield: 0.14 g, 19%. Anal. Calcd for $C_{17}H_{22}Cl_3Cu_2N_4O_5S\cdot 0.5H_2O$ (M_r 636.90): C, 32.06, H, 3.64, N, 8.80, S, 5.03. Found: C, 31.95, H, 3.69, N, 8.59, S, 5.02. Solubility in water: ≥ 9.00 mg/mL. ESI–MS (methanol), positive *m/z* 516 $[Cu^I(HL^6)Cl + Na]^+$, 458 $[Cu^I(HL^6)]^+$. UV–vis (methanol), λ_{max} (ε, $M^{-1}cm^{-1}$): 229 (12744), 259 (16522), 299 (13967), 370 (7692) at 5.2×10^{-5} M, 658 (438) at 1.5×10^{-3} M. ATR–IR, cm^{-1}: 3304w, 3177w, 3026m, 2955w, 2924w, 1726vs, 1622m, 1553s, 1531s, 1427s, 1366s, 1323m, 1294s, 1213vs, 1136vs, 1111s, 987s, 862s, 810m, 775m, 729s, 671m, 609m, 577w.

Crystallographic Structure Determination. X-ray diffraction measurements were performed on Bruker X8 APEXII, Bruker D8 Venture and Oxford Diffraction SuperNova CCD diffractometers. Single crystals of **H_2L^1**–**$H_2L^6\cdot 2H_2O$** were positioned at 35, 24, 35, 24, 24 and 40 mm from the detector, and 512, 1554, 950, 687, 748 and 304 frames were measured, each for 3, 3, 3, 30, 8 and 10 s over 0.5, 0.5, 0.5, 0.5, 0.5 and 1° scan width, respectively. Single crystals of **1·CH_3OH**, **2**, **3**, **4**, **5** and **6·0.5CH_3OH** were positioned at 25, 24, 24, 35, 40 and 24 mm from the detector, and 2647, 1881, 1190, 946, 748 and 1447 frames were measured, each for 24, 30, 4, 10, 60 and 60 s over 0.4, 0.5, 0.5, 0.5, 0.5 and 0.4° scan width, respectively. The data were processed using SAINT software.[52] Crystal data, data collection parameters, and structure refinement details are given in Tables S2 and S3. The structures were solved by direct methods and refined by full-matrix least-squares techniques. Non-H atoms were refined with anisotropic displacement parameters. H atoms were inserted in calculated positions and refined with a riding model. The five-membered pyrrolidine ring in **H_2L^3** was found to be disordered over two positions with s.o.f. 0.50:0.50, respectively. The disorder was resolved with constrained anisotropic displacement parameters using EADP instruction of SHELX-2014, respectively. Disorder with s.o.f 0.60:0.40 in one of the methoxy groups and salicylaldimine moiety was resolved with restrained bond distances and constrained displacement parameters using SADI and EADP instructions of SHELX-2014. The following software programs and computer were

used: structure solution, *SHELXS-97*; refinement, *SHELXL-97*;[53] molecular diagrams, *ORTEP-3*;[54] computer, Intel CoreDuo. CCDC 1522726–1522737.

Powder X-ray Diffraction (XRD) Measurements. Powder XRD was performed on a Bruker D8 diffractometer in Bragg-Brentano reflection geometry using CuK_α radiation and a silicon strip 1-D detector (Lynxeye). A zero-background silicon single crystal sample holder was used. The measurements were done in a $\theta/2\theta$ arrangement, with a variable slit aperture (12 mm illumination on the sample). Analysis of the obtained powder patterns was done by Rietveld refinement with the software program Topas3.

Cell Culture. Human cervix carcinoma cells (HeLa), lung adenocarcinoma cells (A549), colon cancer cells (LS-174) and human foetal lung fibroblast cells (MRC-5) cells were maintained as monolayer culture in the Roswell Park Memorial Institute (RPMI) 1640 nutrient medium (Sigma Chemicals Co, USA), while human myelogenous leukaemia cells (K562) were maintained in suspension culture. RPMI 1640 nutrient medium was prepared in sterile ionized water, supplemented with penicillin (192 U/mL), streptomycin (200 μg/mL), 4-(2-hydroxyethyl)piperazine-1-ethanesulfonic acid (HEPES) (25 mM), l-glutamine (3 mM) and 10 % of heat inactivated foetal calf serum (FCS) (pH 7.2). The cells were grown at 37 °C in 5% CO_2 and humidified air atmosphere, by twice weekly subculture.

MTT Assay. Cytotoxicity of the investigated copper(II) complexes **1**–**6** and the corresponding proligands $\mathbf{H_2L^1}$–$\mathbf{H_2L^6}$ in comparison to cisplatin was determined using the 3-(4,5-dimethylthiazol-2yl)-2,5-diphenyltetrazolium bromide (MTT, Sigma-Aldrich) assay. The MTT colorimetric assay is based on the measurement of mitochondrial enzyme succinate dehydrogenase activity, as an indication of cell viability.[55] Cells were seeded in 96-well cell culture plates (NUNC): HeLa (4000 c/w), A549 (6000 c/w), LS-174 (7000 c/w) and MRC-5 (5000 c/w) in culture medium and grown for 24 h. K562 (5000 c/w) cells were seeded 2 h before treatment. Stock solutions of investigated agents were made in DMSO at concentration of 10 mM, and further diluted with nutrient medium to desired final concentrations (in ranges up to 100 μM). Cisplatin (CDDP) stock solution was made in 0.9% NaCl at concentration of 1.66 mM and diluted with nutrient medium to desired final concentrations (in ranges up to 100 μM). The final concentration of DMSO per well did not exceed 1%. Solutions of various concentrations of examined compounds were added to the wells, except the control wells where only nutrient medium was added. All samples were prepared in triplicates. Nutrient medium

with corresponding agent concentrations but without target cells was used as a blank, also in triplicate.

Cells were incubated for 48 h with the test compounds at 37 °C, with 5% CO_2 in a humidified atmosphere. After incubation, 20 μL of MTT solution, 5 mg/mL in phosphate buffer solution (PBS), pH 7.2, was added to each well. Samples were incubated for 4 h at 37 °C, with 5% CO_2 in humidified atmosphere. Formazan crystals were dissolved in 100 μL 10% sodium dodecyl sulfate (SDS). Absorbance was recorded on the ThermoLabsystems 408 Multiskan EX 200–240 V after 24 h at a wavelength of 570 nm.

Cell Cycle Analysis. Flow cytometric analysis of cell cycle phase distribution of K562 cells treated with copper(II) complexes and cisplatin as a reference compound was performed after staining fixed cells with propidium iodide (PI).[56] Cells were seeded at a density of 2.5×10^5 cells/well in 6-well plates (Thermo Scientific Nunc™), and grown in nutrition medium. After 4 h of stabilization period, K562 cells were continually exposed to complexes **2** and **3**, corresponding proligands (**H_2L^2** and **H_2L^3**) and cisplatin with concentrations corresponding to 1 × IC_{50} (determined for 48 h treatment). After 24 and 48 h of continual treatment, cells were collected, washed twice with ice-cold PBS, and fixed for 30 min in 70% EtOH. After fixation, cells were washed again with PBS, and incubated with RNaseA (1 mg/mL) for 30 min at 37 °C. Cells were than stained with PI (400 μg/mL) for 15 min before flow cytometric analysis. Cell cycle phase distribution was analyzed using a fluorescence activated sorting cells (FASC) Calibur Becton-Dickinson flow cytometer and Cell Quest computer software.

Apoptotic Assay. Flow cytometric analysis of cell death induced by **2** and cisplatin as reference compound, was performed by Annexin V-FITC apoptosis detection kit, according to the manufacturer's instructions (BD Biosciences Cat. No. 65874x, Pharmingen San Diego, CA, USA). K562 cells (2.5×10^5) were seeded into 6-well plates (Thermo Scientific Nunc™), in 2 mL of RPMI medium. After 4 h of stabilization period, cells were treated with **2** or cisplatin with concentrations that correspond to 1 × IC_{50} and 1.5 × IC_{50} (determined for 48 h treatment). After treatment, cells were washed with ice-cold PBS and then resuspended in 200 μL binding buffer (10 mM HEPES/NaOH pH 7.4, 140 mM NaCl, 2.5 mM $CaCl_2$). 100 μL of cell suspension was transferred to a 5-mL culture tube and mixed with 5 μL of Annexin V-FITC and 5 μL of propidium iodide (PI). After incubation for 15 min, at 25 °C in the dark, 400 μL of binding buffer was added to each tube

and analyzed using a FACS Calibur Becton-Dickinson flow cytometer and Cell Quest computer software. A minimum of 10,000 cells were analyzed per sample.

Molecular Modeling. The compounds were docked to the crystal structure of the R2 subunit of RNR (PDBid:1W68)(resolution 2.2 Å),[14b,15] which was obtained from the Protein Data Bank (PDB).[57,58] The Scigress version FJ 2.6 program[59] was used to prepare the crystal structure for docking, i.e., hydrogen atoms were added, the crystallographic water molecules were removed. The software was also used to prepare the compounds for docking using MM2[603] force field or by entering crystallographic co-ordinates. The docking directed at the center of the binding pocket was defined as (x = 102.276, y = 87.568, z = 80.588) with 10 Å radius. One hundred runs were allowed for each compound with 100% search efficiency. The basic amino acids lysine and arginine were defined as protonated. Furthermore, aspartic and glutamic acids were assumed to be deprotonated. The GoldScore (GS),[61] scoring function was implemented to validate the predicted binding modes and relative energies of the ligands using the GOLD v5.4 software suite.

Cloning, Expression and Purification of Mouse R2. Mouse R2 was cloned, expressed and purified based on previous protocols,[62,63] with some modifications. In brief, the *R2* gene synthesized and cloned into a pET-3b plasmid was ordered from GenScript (GenScript USA Inc). The pET-3b-R2 plasmid was transformed into competent *E. coli* BL21 (DE3)-T1^{R} cells (Sigma-Aldrich). Cells containing the pET-3b-R2 plasmid were grown in Terrific Broth (TB) medium containing 100 μg/mL ampicillin. Protein expression was induced by adding isopropyl β-D-1-thiogalactopyranoside (IPTG) to a final concentration of 0.5 mM. Cell cultures expressing the R2 protein were incubated for 12–16 h at 20 °C with vigorous shaking before harvesting. The frozen cell paste was lysed using an X-press®,[64] dissolved in buffer containing 100 mM Tris-HCl, pH 7.5, 10 mM EDTA, 2 mM dithiothreitol (DTT) and protease inhibitor cocktail (Roche), and cleared from nucleic acids by streptomycin sulfate (2.5%) precipitation. Mouse R2 protein was precipitated with 0.29 g/ml ammonium sulfate, dissolved in 50 mM Tris-HCl, pH 7.5, 1 mM DTT and desalted using a HiTrap Desalting column (GE Healthcare). Desalted protein was applied to a HiTrap HP Q column (GE Healthcare), and the proteins were separated with a 0 – 0.5 M KCl gradient. As a final polishing step, the protein was purified on a Superdex 200 column or a Hiload 16/60 Superdex 200 column (GE Healthcare), and stored in 50 mM HEPES, pH 7.5.

Reconstitution of the Tyrosyl Radical in Mouse R2. After purification, R2 protein was treated with 10 mM EDTA and 20 mM hydroxyurea, and passed through a 5 mL HiTrap desalting column (GE Healthcare) to remove iron and to quench the tyrosyl radical (Y•) before reconstitution with Fe(II). For protein sample preparations, unless stated differently, protein reactivation of apo-R2 was performed with addition of excess Fe(II) and O_2, using a solution of $(NH_4)_2Fe(SO_4)_2{\cdot}6H_2O$, pH ~2.3, giving a 7 Fe(II)/R2 dimer ratio.

MST Sample Preparation and Measurements. The binding affinity of both $\mathbf{H_2L^2}$ and complex **3** was tested against mouse R2 protein using Microscale Thermophoresis (MST).[65,66] A concentrated solution of R2 protein was diluted to 500 nM R2 monomer in MST buffer (50 mM Tris-HCl, pH 7.4, 150 mM NaCl, 10 mM $MgCl_2$, and 0.1% pluronic (surfactant used to avoid sample adhesion to the capillaries and tubes)), and reconstituted as described above, however, with an $(NH_4)_2Fe(SO_4)_2{\cdot}6H_2O$ amount giving a 4 Fe(II)/R2 dimer ratio. Concentrated stocks of both compounds, $\mathbf{H_2L^2}$ and **3** (3 mM in DMSO), were diluted to final concentrations of 200 µM in MST buffer containing 10% DMSO, and 1:1 serial dilutions of each compound were prepared. An equal, fixed volume of the reconstituted R2 protein in MST buffer was added to all samples, giving a final concentration of 5% DMSO and 250 nM R2 protein in each sample. The samples were left to incubate for 5 min before they were loaded into standard treated capillaries (Nanotemper Technologies). Data collection was carried out at 25 °C in a Monolith NT.LabelFree apparatus (Nanotemper Technologies). Data was recorded at 20% LED power (and 20 and 40% MST power during testing), and ran in multiple parallels. Data analysis was carried out using MO.Affinity Analysis (Nanotemper Technologies) and Origin softwares (OriginLab Corporation). As specific, ligand-induced changes in fluorescence were observed for both compounds, the changes in fluorescence intensity were directly used to determine binding affinities. The K_Ds were determined in the Origin software (OriginLab Corporation), using a Hill Fitting model option, where the Hill slope was fixed to n = –1.

EPR Sample Preparation. Highly purified mouse R2 protein, reconstituted as described above, was used for incubation with the proligand $\mathbf{H_2L^2}$ and complex **3**. The proligand and complex are soluble in DMSO, and solutions each containing 3 mM $\mathbf{H_2L^2}$ or **3** in DMSO were prepared. The final DMSO concentration in the protein solution was kept to 1%. Two series of samples were prepared and used for separate EPR measurements. For one EPR experiment, three samples of 180 µL 55 µM R2 monomer in 50 mM HEPES, pH 7.5, 100 mM KCl, 1% DMSO and 5% glycerol were prepared,

where two samples were also added $\mathbf{H_2L^2}$ or **3** to final concentrations of 40 µM (yielding a molar ratio of ~ 0.75 tested compound/R2 monomer). For another EPR experiment, three samples of 180 µL 50 µM R2 monomer in 50 mM HEPES, pH 7.5, 100 mM KCl, 1% DMSO and 5% glycerol were prepared, where two samples were also added $\mathbf{H_2L^2}$ or **3** to final concentrations of 50 µM (yielding a molar ratio of 1 tested compound/R2 monomer). All samples were incubated at 298 K for 1 min, transferred to quartz EPR tubes and frozen in liquid nitrogen. During the latter EPR measurements, DTT was added at two different time points (see next section).

X-band EPR Experiments – Quenching of the Y• in the R2 protein. X-band EPR spectra of samples containing mouse R2 protein (blank), and mouse R2 protein added either $\mathbf{H_2L^2}$ or **3** were recorded at 30 K on a Bruker Elexsys 560 EPR spectrometer equipped with an Oxford ESR 900 helium flow cryostat, and a Super X kv319 cavity. All samples contained 5% (v/v) glycerol for vitrification during the low-temperature recordings. EPR spectra were measured at 0.05 mW microwave power and 2 G (0.2 mT) modulation amplitude, quantified by double integration of the spectra recorded under non-saturating conditions, and compared with a standard of 0.2 mM $CuCl_2$ in 1M $HClO_4$. The samples used for kinetic monitoring of the tyrosyl radical concentration were incubated at 298 K for times indicated below, and quickly re-frozen in liquid N_2. In the first set of EPR measurements, spectra were recorded at 30 K after incubating the samples at 298 K for 1, 16, 116, 446, and 1450 min in total. In the second set of EPR measurements, spectra were recorded at 30 K after incubating the samples at 298 K for 1, 6.5, 26, 86, 146, and 1226 min in total. In the latter measurements, 0.5 mM DTT (stock solution pH 7.5) was added after 6.5 min incubation and a second addition of 1 mM DTT (stock solution pH 6.5) was performed after 146 min of incubation at room temperature.

UV–vis Spectroscopy of Mouse R2 with $\mathbf{H_2L^2}$ and 3. The active mouse R2 protein was analyzed at room temperature by UV–vis spectroscopy using an Agilent 8453 diode array ultraviolet-visible spectrophotometer. All spectra were baseline corrected. 30 µM R2 protein in 50 mM HEPES, pH 7.5, was added either $\mathbf{H_2L^2}$ or **3** (in 1% DMSO/50 mM HEPES pH 7.5) at two different times, yielding total concentrations of compounds of 6 and 30 µM, respectively. 1 mM DTT was added twice, yielding a total DTT concentration of 2 mM.

Associated Content

Supporting Information

The Supporting Information is available free of charge on the ACS Publications website at DOI: 10.1021/acs.inorgchem.0000000. X-ray crystallographic data (powder diffraction and single crystal), IR spectra, ^{1}H and ^{13}C NMR spectra.

Author Information

Corresponding Author

*For V.B.A.: phone, +43 1 4277 52615; E-mail, vladimir.arion@univie.ac.at.

Acknowledgments. We thank Alexander Roller for collection of X-ray data. MZ and VBA are indebted to the Austrian Science Fund (FWF) for support of this work by grant no. P28223-N34 (to V.B.A), and KKA to the Research Council of Norway for support of this work by grant no. 214239. The MST instrument was operated with the financial support of the South-Eastern Norway Regional Health Authority (grant no. 2015095; Regional Core Facility for Structural Biology).

References

1. (a) Donnelly, P. S. The role of coordination chemistry in the development of copper and rhenium radiopharmaceuticals. *Dalton Trans.* **2011**, *40*, 999–1010; (b) Lobana, T. S.; Sharma, R.; Bawa, G.; Khanna, S. Bonding and structure trends of thiosemicarbazone derivatives of metals – an overview. *Coord. Chem. Rev.* **2009**, *253*, 977–1055; (c) Sadimenko, A. P. Organometallic complexes of pyridyl Schiff bases. *Adv. Heterocyclic Chem.* **2012**, *107*, 133–218.

2. (a) Beraldo, H.; Gambino, D. The wide pharmacological versatility of semicarbazones, thiosemicarbazones and their metal complexes. *Mini-Rev. Med. Chem.* **2004**, *4*, 31–39; (b) Reis, D. C.; Despaigne, A. A. R.; Da Silva, J. G.; Silva, N. F.; Vilela, C. F.; Mendes, I. C.; Takahashi, J. A.; Beraldo, H. Structural studies and investigation on the activity of imidazole-derived thiosemicarbazones and hydrazones against crop-related fungi. *Molecules* **2013**, *18*, 12645–12662.

3. (a) Ravina, E. The evolution of drug discovery: from traditional medicines to modern drugs. Weinheim: Wiley-VCH, 2011; (b) Dilworth, J. R.; Hueting, R. Metal complexes of thiosemicarbazones for imaging and therapy. *Inorg. Chim,. Acta* **2012**, *389*, 3–15.

4. Finch, R. A.; Liu, M.; Grill, S. P.; Rose, W. C.; Loomis, R.; Vasquez, K. M.; Cheng, Y.; Sartorelli, A. C. Triapine (3-aminopyridine-2-carboxaldehyde-thiosemicarbazone): a potent inhibitor of

ribonucleotide reductase activity with broad spectrum of antitumor activity. *Biochem. Pharmacol.* **2000**, *59*, 983–991.

5. Traynor, A. M.; Lee, J. W.; Bayer, G. K.; Tate, J. M.; Thomas, S.; Mazurczak, M.; Graham, D. L.; Kolesar, J. M.; Schiller, J. H. A phase II trial of triapine (NSC# 663249) and gemcitabine as second line treatment of advanced non-small cell lung cancer: Eastern Cooperative Oncology Group Study 1503. *Invest. New Drugs* **2010**, *28*, 91–97.

6. Knox, J. J.; Hotte, S. J.; Kollmannsberger, C.; Winquist, E.; Fisher, B.; Eisenhauer, E. A. Phase II study of triapine in patients with metastatic renal cell carcinoma: a trial of the National Cancer Institute of Canada Clinical Trials Group (NCIC IND.161). *Invest. New Drugs* **2007**, *25*, 471–477.

7. Odenike, O. M.; Larson, R. A.; Gajria, D.; Dolan, M. E.; Delaney, S. M.; Karrison, T. G.; Ratain, M. J.; Stock, W. Phase I study of the ribnucleotide reductase inhibitor 3-aminopyridine-2-carboxaldehyde-thiosemicarbazone (3-AP) in combination with high dose cytarabine in patients with advanced myeloid leukemia. *Invest. New Drugs* **2008**, *26*, 233–239.

8. Karp, J. E.; Giles, F. J.; Gojo, I.; Morris, L.; Greer, J.; Johnson, B.; Thein, M.; Sznol, M.; Low, J. A phase I study of the novel ribnucleotide reductase inhibitor 3-aminopyridine-2-carboxaldehyde-thiosemicarbazone (3-AP, triapine) in combination with the nucleoside analog fludarabine for patients with refractory acute leukemias and aggressive myeloproliferative disorders. *Leuk. Res.* **2008**, *32*, 71–77.

9. Attia, S.; Kolesar, J.; Mahoney, M. R.; Pitot, H. C.; Laheru, D.; Heun, J.; Huang, W.; Eickhoff, J.; Erlichman, C.; Holen, K. D. A phase 2 consortium (P2C) trial of 3-aminopyridine-2-carboxaldehyde-thiosemicarbazone (3-AP) for advanced adenocarcinoma of the pancreas. *Invest. New Drugs* **2008**, *26*, 369–379.

10. Kowol, C. R.; Miklos, W.; Pfaff, S.; Hager, S.; Kallus, S.; Pelivan, K.; Kubanik, M.; Enyedy, E. A.; Berger, W.; Heffeter, P.; Keppler, B. K. Impact of stepwise NH_2-methylation of triapine on the physico-chemical properties, anticancer activity and resistance circumvention. *J. Med. Chem.* **2016**, *59*, 6739–6752.

11. Nordlund, N.; Reichard, P. Ribonucleotide reductases. *Annu. Rev. Biochem.* **2006**, *75*, 681–706.

12. Tomter, A. B.; Zoppellaro, G.; Andersen, N. H.; Hersleth, H. P.; Hammerstad, M.; Rohr, A. K.; Sandvik, G. K.; Strand, K. R.; Nilsson, G. E.; Bell, C. B.; Barra, A. L.; Blasco, E.; Le Pape, L.; Solomon, E. I.; Andersson, K. K. *Coord. Chem. Rev.* **2013**, 257, 3–26.

13. Shao, J.; Zhou, B.; Chu, B.;Yen, Y. Ribonucleotide reductase inhibitors and future drug design. *Curr. Cancer Drug Targets* **2006**, *6*, 409–431.

14. (a) Aye, Y.; Long, M. J. C.; Stubbe, J. Mechanistic studies of semicarbazone Triapine targeting human ribonucleotide reductase *in vitro* and in mammalian cells. *J. Biol. Chem.* **2012**, *287*, 35768–35778; (b) Popovic-Bijelic, A.; Kowol, C.R.; Lind, M.; Luo, J.; Himo, F.; Enyedy, E.A.; Arion, V.B.; Gräslund, A. Ribonucleotide reductase inhibition by metal complexes of 3-aminopyridine-2-carboxaldehyde thiosemicarbazone (triapine): a combined experimental and theoretical study. *J. Inorg. Biochem.* **2011**, *105*, 1422–1431.

15. Strand, K. R.; Karlsen, S.; Kolberg, M.; Røhr, A. K.; Görbitz, C. H.; Andersson, K. K. Crystal structural studies of changes in the native dinuclear iron center of ribonucleotide reductase protein R2 from mouse. *J. Biol. Chem.* **2004**, *279*, 46794–46801.

16. https://clinicaltrials.gov/ct2/show/NCT02433626.

17. Stacy, A. E.; Palanimuthu, D.; Bernhardt, P. V.; Kalinowski, D. S.; Jansson, P. J.; Richardson, D. R. Zinc(II)-thiosemicarbazone complexes are located to the lysosomal compartment where they transmetallate with copper ions to induce cytotoxicity. *J. Med. Chem.* **2016**, *59*, 4965–4984.

18. Salim, K. Y.; Vareki, S. M.; Danter, W. R.; Koropatnik, J. COTI-2, a novel small molecule that is active against multiple human cancer cell lines *in vitro* and *in vivo*. *Oncotarget* **2016**, *7*, 41363–41379.

19. (a) Omuro, A.; DeAngelis, L. M. Glioblastoma and other malignant gliomas: a clinical review. *Jama* **2013**, *310*, 1842–1850; (b) Siddik, Z. H. Cisplatin: mode of cytotoxic action and molecular basis of resistance. *Oncogene* **2003**, *22*, 7265–7279.

20. Bota, D. A.; Desjardins, A.; Quinn, J. A.; Affronti, M. L.; Friedman, H. S. Interstitial chemotherapy with biodegradable BCNU (Gliadel) wafers in the treatment of malignant gliomas. *Therapeutics and clinical risk management* **2007**, *3*, 707–715.

21. Maione, P.; Rossi, A.; Bareschino, M.; Sacco, P. C.; Schettino, C.; Casaluce, F.; Sgambato, A.; Gridelli, C. Irreversible EGFR inhibitors in the treatment of advanced NSCLC. *Curr. Pharm. Des.* **2014**, *20*, 3894–3900.

22. Lovejoy, D. B.; Sharp, D. M.; Seebacher, N.; Obeidy, P.; Prichard, T.; Stefani, C.; Basha, M. T.; Sharpe, P. C.; Jansson, P. J.; Kalinowski, D. S.; Bernhardt, P. V.; Richardson, D. R. Novel second generation di-2-pyridylketone thiosemicarbazones show synergism with standard chemotherapeutics and demonstrate potent activity against lung cancer xenografts after oral and intravenous administration in vivo. *J. Med. Chem.* **2012**, *55*, 7230–7244.

23. Stacy, A. E.; Palanimuthu, D.; Bernhardt, P. V.; Kalinowski, D. S.; Jansson, P. J.; Richardson, D. R. Structure–activity relationships of di-2-pyridylketone, 2-benzoylpyridine, and 2-acetylpyridine

thiosemicarbazones for overcoming Pgp-mediated drug resistance. *J. Med. Chem.* **2016**, *59*, 8601–8620.

24. Patiño, O. J.; Cuca, L. E. Monophyllidin, a new alkaloid L-proline derivative from *Zanthoxylum monophyllum*. *Phytochem. Lett.* **2011**, *4*, 22–25.

25. Hamre, D.; Bernstein, J.; Donovick, R. Activity of *p*-aminobenzaldehyde 3-thiosemicarbazone on vaccine virus in the chick embryo and in the mouse. *Exp. Biol. Med.* **1950**, *73*, 275–278.

26. Brownlee, K. A.; Hamre, D. Studies on chemotherapy of vaccinia virus. I. An experimental design for testing antiviral agents. *J. Bacteriol.* **1951**, *61*, 127–134.

27. Milunovic, M. N. M.; Enyedy, É. A.; Nagy, N. V.; Kiss, T.; Trondl, R.; Jakupec, M. A.; Keppler, B. K.; Krachler, R.; Novitchi, G.; Arion, V. B. L- and D-proline thiosemicarbazone conjugates: coordination behaviour in solution and the effect of copper(II) coordination on their antiproliferative activity. *Inorg. Chem.* **2012**, *51*, 9309–9321.

28. Bacher, F.; Dömötör, O.; Kaltenbrunner, M.; Mojovic, M.; Popović-Bijelić, A.; Gräslund, A.; Ozarowski, A.; Filipović, L.; Radulović, S.; Enyedy, É. A.; Arion, V. B. Effects of terminal dimethylation and metal coordination of proline-2-formylpyridine thiosemicarbazone hydrids on lipophilicity, antiproliferative activity and hR2 RNR inhibition. *Inorg. Chem.* **2014**, *53*, 12595–12609.

29. Bacher, F.; Enyedy, É. A.; Nagy, N.V.; Rockenbauer, A.; Bognár, G. M.; Trondl, R.; Novak, M. S.; Klapproth, E.; Kiss, T.; Arion, V. B. Copper(II) complexes with highly water-soluble L- and D-proline-thiosemicarbazone conjugates as potential inhibitors of topoisomerase IIα. *Inorg. Chem.* **2013**, *52*, 8895–8908.

30. Yu, Y.; Kalinowski, D. S.; Kovacevic, Z.; Siafarkas, A. R.; Jansson, P. J.; Stefani, C.; Lovejoy, D. B.; Sharpe, P. C.; Bernhardt, P. V.; Richardson, D. R. Thiosemicarbazones from the old to new: iron chelators that are more than just ribonucleotide reductase inhibitors. *J. Med. Chem.* **2009**, *52*, 5271–5294.

31. Ni, L.; Wang, J.; Liu, C.; Fan, J.; Sun, Y.; Zhou, Z.; Diao, G. An asymmetric binuclear zinc(II) complex with mixed iminodiacetate and phenanthroline ligands: synthesis, characterization, structural conversion and anticancer properties. *Inorg. Chem. Front.* **2016**, *3*, 959–968.

32. (a) Pate J. E., Cruse R. W.; Karlin, K. D.; Solomon, E- I. Vibrational, electronic and resonance Raman spectral studies of $[Cu_2(YXL\text{-}O\text{-})O_2]^+$, a copper(II) peroxide model complex of oxyhemocyanin. *J. Am. Chem. Soc*. **1987**, 109, 2624–2630. (b) Op't Holt, B. T.; Vance, M. A.; Mirica, L. M.; Heppner, D. E.; Stack, T. D. P.; Solomon, E. I. Reaction coordinate of a functional

model of tyrosinase: spectroscopic and computational characterization. *J. Am. Chem. Soc.* **2009**, *131*, 6421–6438; (c) Jazdzewski, B. A.; Tolman, W. B. Understanding the copper-phenoxyl radical array in galactose oxidase: contributions from synthetic modeling studies. *Coord. Chem. Rev.* **2000**, *200–202*, 633–685; (d) Jazdzewski, B. A.; Reynolds, A. M.; Holland, P. L.; Young, V. G.; Kaderli, S.; Zuberbuhler, A. D.; Tolman, W. B. Copper(I)-phenolate complexes as models of the reduced active site of galactose oxidase: synthesis, characterization, and O_2 reactivity. *J. Biol. Inorg. Chem.* **2003**, *8*, 381–393; (e) Hanson, M. A.; Schmidt, P. P.; Strand, K. R.; Gräslund, A.; Solomon, E. I.; Andersson, K. K. Resonance Raman evidence for a hydrogen-based oxo-bridge in the R2 protein of ribonucleotide reductase from mouse. *J. Am. Chem. Soc.* **1999**, *121*, 6755–6756; (f) Schmidt, P. P.; Andersson, K. K.; Barra, A.-L.; Thelander, L.; Gräslund, A. High field EPR studies of mouse ribonucleotide reductase indicate hydrogen bonding of the tyrosyl radical. *J. Biol. Chem.* **1996**, *271*, 23615–23618.

33. Primik, M. F., Göschl, S., Meier, S. M., Eberherr, N., Jakupec, M. A., Enyedy, E. A., Novitchi, G., Arion, V. B. Dicopper(II) and dizinc(II) complexes with nonsymmetric dinucleating ligands based on indolo[3,2-*c*]quinolines: synthesis, structure, cytotoxicity, and intracellular distribution. *Inorg.Chem.* **2013**, *52*, 10137–10146.

34. Eaborn, C. Cleavages of aryl-silicon and related bonds by electrophiles. *J. Organomet. Chem*. **1975**, *100*, 43−57.

35. Silverman, G.; Rakita, P. E. *Handbook of Grignard Reagents*, CRC Press, 25 apr. 1996, pp. 659−660 and references cited therein.

36. Gilman, H.; Brook, A. G.; Miller, L. S. The alkaline cleavage of tetrasubstituted silanes. *J. Am. Chem. Soc.* **1953**, *75*, 4531−4534.

37. Schmidt, H. M.; Arens, J. F. Cleavage of the carbon-silicon bond in 1-alkynyl-silanes by silver nitrate. *RECUEIL* **1967**, *86*, 1138−1142.

38. Valk, J.-M.; Boersma, J.; van Koten, G. Selective intramolecular cleavage of the carbon-silicon bond by palladium salts, *J. Organometal. Chem.* **1994**, *483*, 213−216.

39. Pola, S. *Significance of Thiazole-based Heterocycles for Bioactive Systems, Chapter 1 in: Scope of Selective Heterocycles from Organic and Pharmaceutical Perspective*, Ed. by Ravi Varala, InTech, doi: 10.5772/62077.

40. Addison, A. W.; Rao, T. N.; Reedijk, J.; van Rijn, J.; Verschoor, G. C. Synthesis, structure and spectroscopic properties of copper(II) compounds containing nitrogen-sulphur donor ligands; the

crystal and molecular structure of aqua[1,7-*bis*(*N*-methylbenzimidazol-2'-yl)-2,6-dithiaheptane]copper(II) perchlorate. *J. Chem. Soc. Dalton Trans*. **1984**, 1349–1356.

41. Gerbeleu, N. V.; Arion, V. B.; Burgess, J. Template Synthesis of Macrocyclic Compounds. Wiley-VCH, Weinheim, 1999.

42. Rogolino, D.; Cavazzoni, A.; Gatti, A.; Tegoni, M.; Pelosi, G.; Verdolino, V.; Fumarola, C.; Cretelola, D.; Petronini, P. G.; Carcelli, M. Anti-proliferative effects of copper(II) complexes with hydroxyquinoline-thiosemicarbazone ligands. *Eur. J. Med. Chem.* **2017**, *128*, 140–153.

43. Saswati, Chakraborty, A.; Dash, S. P.; Panda, A. K.; Acharyya, R.; Biswas, A.; Mukhopadhyay, S.; Bhutia, S. K.; Crochet, A.; Patil, Y. P.; Nethaji, M.; Dinda, R. Synthesis, X-ray structure and in vitro cytotoxicity of Cu(I/II) complexes of thiosemicarbazone: special emphasis on their interactions with DNA. *Dalton Trans.* **2015**, *44*, 6140–6157.

44. Zhang, Z.; Gou, Y.; Wang, J.; Yang, K.; Qi, J.; Zhou, Z.; Liang, S.; Liang, H.; Yang, F. Four copper(II) compounds synthesized by anion regulation: Structure, anticancer function and anticancer mechanism. *Eur. J. Med. Chem.* **2016**, *121*, 399–409.

45. Qi, J.; Liang, S.; Gou, Y.; Zhang, Z.; Zhou, Z.; Yang, F.; Liang, H. Synthesis of four binuclear copper(II) complexes: Structure, anticancer properties and anticancer mechanism. *Eur. J. Med. Chem.* **2015**, *96*, 360–368.

46. Liu, Y.-H.; Li, A.; Shao, J.; Xie, C.-Z.; Song, X.-Q.; Bao, W.-G.; Xu, J.-Y. Four Cu(II) complexes based on antitumor chelators: synthesis, structure, DNA binding/damage, HSA interaction and enhanced cytotoxicity. *Dalton Trans.* **2016**, *45*, 8036–8049.

47. Sobiesiak, M.; Cieslak, M.; Krolewska, K.; Kazmierczak-Baranska, J.; Pasternak, B.; Budzisz, E. Thiosemicarbazone-derived copper(II), cobalt(II) and nickel(II) complexes as potential anticancer agents: nuclease activity, cytotoxicity and apoptosis studies. *New J. Chem.* **2016**, *40*, 9761–9767.

48. Ormerod, M. G. Analysis of DNA-general methods. In: Ormerod MG (ed) Flow cytometry, a practical approach. Oxford University Press, New York, 1994, pp 119–125.

49. Jerabek-Willemsen, M.; Andre, T.; Wanner, R.; Roth, H. M.; Duhr, S.; Baaske, P.; Breitsprecher, D. MicroScale Thermophoresis: Interaction analysis and beyond. *J. Mol. Struct.* **2014,** 1077, 101–113.

50. Kowol, C. R.; Berger, R.; Eichinger, R.; Roller, A.; Jakupec, M. A.; Schmidt, P. P.; Arion, V. B.; Keppler, B. K. Gallium(III) and iron(III) complexes of α-*N*-heterocyclic thiosemicarbazones: Synthesis, characterization, cytotoxicity, and interaction with ribonucleotide reductase. *J. Med. Chem.* **2007**, *50*, 1254–1265.

51. (a) Mylonas, S.; Mamalis, A. Synthesis and antitumor activity of new thiosemicarbazones of 2-acetylimidazo[4,5-*b*]pyridine. *J. Heterocycl. Chem.* **2005**, 42, 1273–1281; (b) Freund, M.; Paradies, Th. Zur Kenntniss des Tetrazols. *Ber. dtsch. chem. Ges.* **1901**, *34*, 3110–3122; (c) Basu, A.; Das, G. Oxydative cyclization of thiosemicarbazones: an optical and turn-on fluorescent chemodosimeter for Cu(II). *Dalton Trans.* **2011**, *40*, 2837–2843. (c) Hassaan, A. M. A., Soliman, E. M., El-Roudi, A. M., Adduct formation by nickel(II) complexes of S-methyl hydrazine carbodithioate Schiff bases with 2,2´-bipyridyl and 1,10-phenanthroline. *Polyhedron*, 1989, **8**, 925–927.

(52) *SAINT-Plus*, version 7.06a and APEX2; Bruker-Nonius AXS Inc.: Madison, WI, 2004.

(53) Sheldrick, G. M. A short history of SHELX. *Acta Crystallogr.* **2010**, *A46*, 112–122.

(54) Johnson, G. K. Report ORNL-5138; OAK Ridge National Laboratory; Oak Ridge, TN, 1976.

(55) Supino, R. Methods in molecular biology. In: O'Hare S, Atterwill CK (eds) In vitro toxicity testing protocols. Humana Press, New Jersey, 1995, pp 137–149.

56. Ormerod, M. G Analysis of DNA-general methods. In: Ormerod MG (ed) Flow cytometry, a practical approach. Oxford University Press, New York, 1994, pp 119–125.

57. Berman, H. M.; Westbrook, J.; Feng, Z.; Gilliland, G.; Bhat, T. N.; Weissig, H.; Shindyalov, I. N.; Bourne, P. E., The Protein Data Bank. *Nuc.Acids Res.* **2000,** *28*, 235–242.

58. Berman, H.; Henrick, K.; Nakamura, H., Announcing the worldwide Protein Data Bank. *Nat. Struct. Biol.* **2003,** *10*, 980.

59. *Scigress Explorer Ultra Version 7.7.0.47*, Fijitsu Limited: 2000 - 2007.

60. Allinger, N. L. Conformational analysis. 130. MM2. A hydrocarbon force field utilizing V1 and V2 torsional terms. *J. Am. Chem. Soc.* **1977**, *99*, 8127–8134.

61. Jones, G.; Willet, P.; Glen, R. C.; Leach, A. R.; Taylor, R., Development and Validation of a Genetic Algorithm for Flexible Docking. *J.Mol.Biol.* **1997,** *267*, 727–748.

(62) Mann, G. J.; Graslund, A.; Ochiai, E. I.; Ingemarson, R.; Thelander, L. Purification and characterization of recombinant mouse and herpes-simplex virus ribonucleotide reductase R2 subunit. *Biochemistry* **1991,** *30*, 1939–1947.

(63) Davis, R.; Thelander, M.; Mann, G. J.; Behravan, G.; Soucy, F.; Beaulieu, P.; Lavallee, P.; Graslund, A.; Thelander, L. Purification, characterization and localization of subunit interaction area of recombinant mouse ribonucleotide reductase R1 subunit, *J. Biol. Chem.* **1994,** *269*, 23171–23176.

64. Magnusson, K. E.; Edebo, L. Influence of cell concentration, temperature and press performance on flow characteristics disintefration in freeze-pressing of *Saccharomyces-cerevisiae* with X-press. *Biotechnology and Bioengineering* **1976**, *18*, 865–883.

(65) Duhr, S.; Braun, D. Why molecules move along a temperature gradient. *Proc. Nat. Acad. Sci. USA* **2006**, *103*, 19678−19682.

(66) Seidel, S. A. I.; Dijkman, P. M.; Lea, W. A.; van den Bogaart, G.; Jerabek-Willemsen, M.; Lazic, A.; Joseph, J. S.; Srinivasan, P.; Baaske, P.; Simeonov, A.; Katritch, I.; Melo, F. A.; Ladbury, J. E.; Schreiber, G.; Watts, A.; Braun, D.; Duhr, S. Microscale thermophoresis quantifies biomolecular interactions under previously challenging conditions. *Methods* **2013**, *59*, 301−315.

Table of Contents

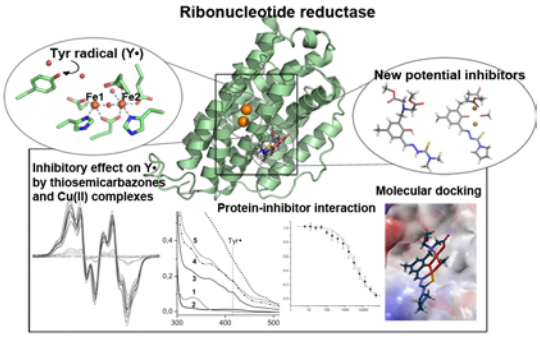

Our findings suggest that some of the synthesized proligands and dicopper(II) complexes are effective antiproliferative agents with selectivity for cancer cells. Molecular modeling calculations, binding affinity measurements performed by microscale thermophoresis, as well as kinetic measurements of the concentration of tyrosyl radical both in the absence and in the presence of DTT by EPR and UV–vis spectroscopies indicate the formation of adducts and possible inhibition of RNR R2 by the investigated compounds.